Journal of Nondestructive Evaluation, Vol. 13, No. 3, 1994

Backscattered Microstructural Noise in Ultrasonic Toneburst Inspections

F. J. Margetan,[1] R. B. Thompson,[1] and I. Yalda-Mooshabad[1]

Received November 29, 1993; revised July 22, 1994

A model is presented which relates the absolute backscattered noise level observed in an ultrasonic immersion inspection to details of the measurement system and properties of the metal specimen under study. The model assumes that the backscattered noise signal observed for a given transducer position is an incoherent superposition of echoes from many grains. The model applies to normal-incidence, pulse-echo inspections of weakly-scattering materials using toneburst pulses from either a planar or focused transducer. The model can be used in two distinct ways. Measured noise echoes can be analyzed to deduce a "Figure-of-Merit" (FOM) which is a property of the specimen alone, and which parameterizes the contribution of the microstructure to the observed noise. If the FOM is known, the model can be used to predict the absolute noise levels that would be observed under various inspection scenarios. Tests of the model are reported, using both synthetic noise echoes, and measured noise echoes from metal specimens having simple and complicated microstructures.

KEY WORDS: Ultrasonics; backscattering; noise; backscatter coefficient; figure-of-merit; microstructure.

1. INTRODUCTION

Ultrasound is often the preferred inspection tool for metals because of its ability to penetrate to the interior of a component. However, sound energy reflected from microstructural features, such as grain boundaries, produces background "noise" which is seen even when no defects are present. This noise can inhibit the detection of a small defect, or of a subtle one, such as an inclusion which has an acoustic impedance similar to that of the host metal in which it resides. Algorithms for estimating the probability of detecting such defects with a given inspection system require quantitative models for microstructural noise levels.

Certain general features of backscattered noise have been known for a long time. For example, it is known that at low frequency the scattering cross-section of a single grain of a polycrystal and the attenuation of a wave propagating through the polycrystal each vary as the fourth power of the frequency[1], and that this behavior is intimately related to that of the backscattered noise.[2] The rate of decay of noise signals with depth has been studied as a means for determining ultrasonic attenuation and other material properties. Important pioneering work was done by Goebbels,[2] who demonstrated the ability to infer grain size from backscattered noise data. Tittmann and Ahlberg[3] studied attenuation and noise in nickel alloys, and demonstrated the important contribution that can be made by microporosity. In the context of developing techniques to measure porosity in cast aluminum, Nagy, Adler, and Rypien[4,5] studied the relationship between the attenuation deduced from backscattered noise, and that deduced from coherent surface echoes, and demonstrated fundamental differences between the two. Until recently there has been relatively little effort devoted toward quantitative study of *absolute* noise levels, as needed to make detectability predictions. Such predictions require an understanding of the dependence of the observed noise on the measurement system, in addition to its dependence on the specimen under

[1] Center for Nondestructive Evaluation, Iowa State University, Ames, Iowa 50011.

0195-9298/94/0900-0111$07.00/0

study. One notable exception is the work of Madsen *et al.*[6–8] in which the observed power spectrum of the noise from a distributed collection of scatterers is related to the incident ultrasonic field and to a "backscatter coefficient" which is a property of the specimen alone. They demonstrated their technique by using measured noise echoes to deduce the backscatter coefficient for a distribution of small glass spheres in a tissue-mimicking medium. An analogous approach was used by Margetan *et al.*[9,10] to analyze the backscattered microstructural noise observed in focused-beam, toneburst inspections of metals. They directly modeled the measurement process, and related the absolute noise level to properties of the measurement system and the metal specimen. Aspects of their model were validated by noise measurements in two-phase titanium alloys. A similar approach, in which the microstructure's backscatter coefficient is related to the noise power spectrum, and the contribution of the measurement system is directly modeled, has been pursued by Russell and Neal.[11–14] Their approach has been demonstrated using backscattered noise echoes from incident longitudinal and shear wave beams in a specimen of pure titanium metal.

For a given inspection methodology, the observed backscattered noise level will depend intimately upon both the material properties of the host metal, and details of the measurement system. We present a model of the noise measurement process which accounts for both types of effects. Rather than treating the noise power spectrum as the measured quantity of interest (which requires Fourier transform operations on noise waveforms during data analysis), we choose to focus on a simple time-domain characterization of the noise. In particular, our model predicts the average absolute noise voltage level as a function of time, or, equivalently, as a function of depth in the specimen. More specifically, at a given time instant, the predicted noise level is the rms (root-mean squared) average of the noise voltage over many independent ensembles of grains, i.e., over independent lateral positions of the transducer. The contribution of the specimen's microstructure to the observed noise level is principally contained in a factor that depends, for single-phase alloys, on the number density of grains and on the rms average plane-wave scattering amplitude of a single grain. This factor is referred to as the Figure-of-Merit (FOM) for the inherent noise severity of the specimen, and is equivalent to the square root of the backscatter coefficient cited by Madsen or Russell. Our model may be used in two distinct ways. If the specimen FOM is unknown, the model can be used to determine its value from measured backscattered noise data. Alternatively, if the FOM is known, the model can be used to predict the rms noise level for different choices of the inspection scenario, e.g., for different choices of the transducer radius, focal length, and inspection waterpath. The version of the model described in the present work applies specifically to normal-incidence, pulse-echo, immersion inspections of weakly scattering materials through planar interfaces when ultrasonic toneburst pulses are used. However, the underlying generic model can be extended to cover oblique-incidence, broadband pulses, and/or curved interfaces.

In Section 2 of the present work we describe the measurement of noise signals and their subsequent analysis to extract the average quantity $N_{rms}(t)$ which characterizes the noise severity at a time t after the front-surface echo. In Section 3 we derive a formula for $N_{rms}(t)$ in weakly-scattering materials, and we indicate how model quantities pertaining to the incident ultrasonic field in the metal are evaluated in practice. In Section 4, we discuss how the time-dependence of $N_{rms}(t)$ is controlled by the depth dependence of the transducer's radiation pattern in the metal, and we explain the peak in $N_{rms}(t)$ that is often observed when a focused transducer is used and t is near the round-trip travel time to the focal zone. In the ensuing two sections various tests of the model are presented, first using synthetic noise echoes, and then using noise echoes measured in a titanium alloy specimen. In the latter case, we use the model to extract the FOM from the measured noise, and we demonstrate that the result is approximately independent of the toneburst duration, the transducer used, or the time (depth) at which the extraction is performed. The FOM extraction procedure assumes knowledge of the effective ultrasonic attenuation of the specimen at the inspection frequency. Three methods for determining this attenuation are discussed and demonstrated in Section 7. For specimens having single-phase, equi-axed microstructures with randomly oriented grains, it is possible to directly estimate the FOM from knowledge of the grain size distribution and the single-crystal elastic constants. In Section 8, for several metal specimens with simple microstructures, we compare such metallographically-determined FOM estimates with values deduced from our model-based analysis of backscattered noise data. FOM values deduced from noise data are reported in Section 9 for four specimens of titanium alloy, of the type used in rotating jet-engine components. There the FOM, and hence the absolute noise level, is often found to be strongly dependent on the direction of sound propagation. In the final section we summarize our findings, indicate how model extensions can be effected, and discuss how the model can be used to predict the likely signal-to-noise ratio when a defect is present during

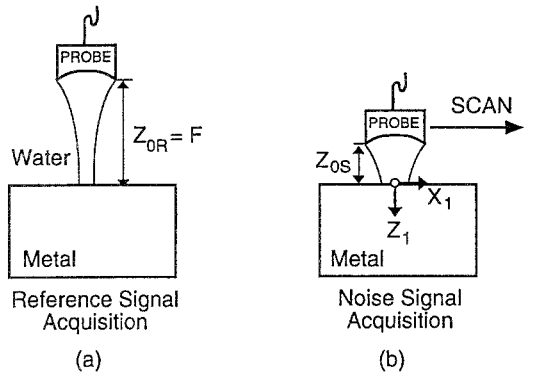

Fig. 1. Transducer positioning for acquisition of (a) front-surface reference signal, and (b) backscattered noise signals.

inspection. The reader desiring a more detailed accounting of the grain-noise investigations reported herein may consult the lengthy summary report which we prepared for our sponsoring agency.[15]

2. MEASUREMENT AND ANALYSIS OF BACKSCATTER GRAIN NOISE

The normal-incidence transducer/specimen geometry addressed by our model is shown in Fig. 1. A pulsing unit (MATEC 6600 or Panametrics 5052PR) supplied an initial voltage pulse to the transducer, resulting in the generation of an ultrasonic pulse traveling toward a submerged metal specimen. Sound echoes, arising from reflection at the front (i.e., top) surface of the specimen and from grain scattering in the interior, returned to the transducer at later times. The returning sound echoes were converted to electrical voltage signals by the piezoelectric element, amplified, and input to a LeCroy 4300 digitizing oscilloscope. Digitized waveforms, sampled at a frequency of 100 MHz, were sent to a computer for storage and subsequent analysis. Both planar and spherically-focused transducers were used, with oscillation frequencies ranging from 5 to 20 MHz. In most cases, auxiliary beam profile measurements[15,16] were performed to estimate the effective element radius (a) and geometric focal length in water (F) of each transducer. In some cases, the a and F values estimated by this procedure differed substantially from those provided by the transducer manufacturer.

At the beginning of each experimental trial, a "reference" echo from the front surface (FS) of the specimen was acquired and stored for later use in re-scaling the noise data. This reference echo, which plays an important role in the model-based analysis of the noise data, serves to encode amplification settings, pulse frequency and duration, and the efficiency of the transducer. When a focused transducer was used, as was generally the case, the waterpath for the reference signal (z_{0R}) was set equal to the geometric focal length (F). This choice was made to simplify the evaluation of a diffraction integral which appears in a subsequent model expression for the reference signal. After reference signal acquisition, the waterpath was shortened (z_{0S}) to focus the beam in the interior of the specimen. With the waterpath fixed, the transducer was scanned above the specimen in the x and y directions, and noise echoes were acquired at each of several hundred transducer positions. At each position, 100 or 200 separate waveforms were acquired and averaged to reduce electronic noise. The same procedure was followed for planar transducers, except that a common waterpath was used for both reference and noise signals, chosen (when practical) such that the specimen was in the far-field zone of the transducer's radiation pattern.

The metal specimens studied were primarily samples of Ti-6246 (i.e., Ti-6%Al-2%Sn-4%Zn-6%Mo) supplied to us by jet engine manufacturers.[17] These specimens possessed two-phase microstructures containing hexagonal (alpha-phase) and cubic (beta-phase) crystallites. For certain aspects of the model validation work, other specimens possessing single-phase microstructures were studied. These included copper, stainless steel, and pure (alpha-phase) titanium specimens with equi-axed, randomly-oriented grains. All specimens were machined into rectangular blocks, and polished with 600-grit or finer sandpaper prior to insonification. For the majority of the Ti-6246 specimens, the level of backscattered noised was observed to be strongly dependent on the direction of beam propagation; thus, it was important to number the faces of each specimen and to record the entry surface for each experiment. Three mutually-orthogonal faces were enumerated 1,2, and 3, and the three opposite faces were enumerated 4,5, and 6, respectively. Complete details of all specimens studied, including dimensions, densities, soundspeeds in the orthogonal directions, and photographs of the microstructures, may be found in Ref. 15.

Notice the coordinate naming conventions used in Fig. 1. Subscripts 0 and 1 refer to water and metal respectively, and subscripts R and S denote the reference and noise-signal geometries. The origin of the (x_1,y_1,z_1) coordinate system in the metal is the entry point of the center of the ultrasonic beam. When displaying either time-domain grain-noise echoes or average noise levels, the time origin (t=0) is chosen at the center of the observed front-surface echo (when the waterpath is z_{0S}).

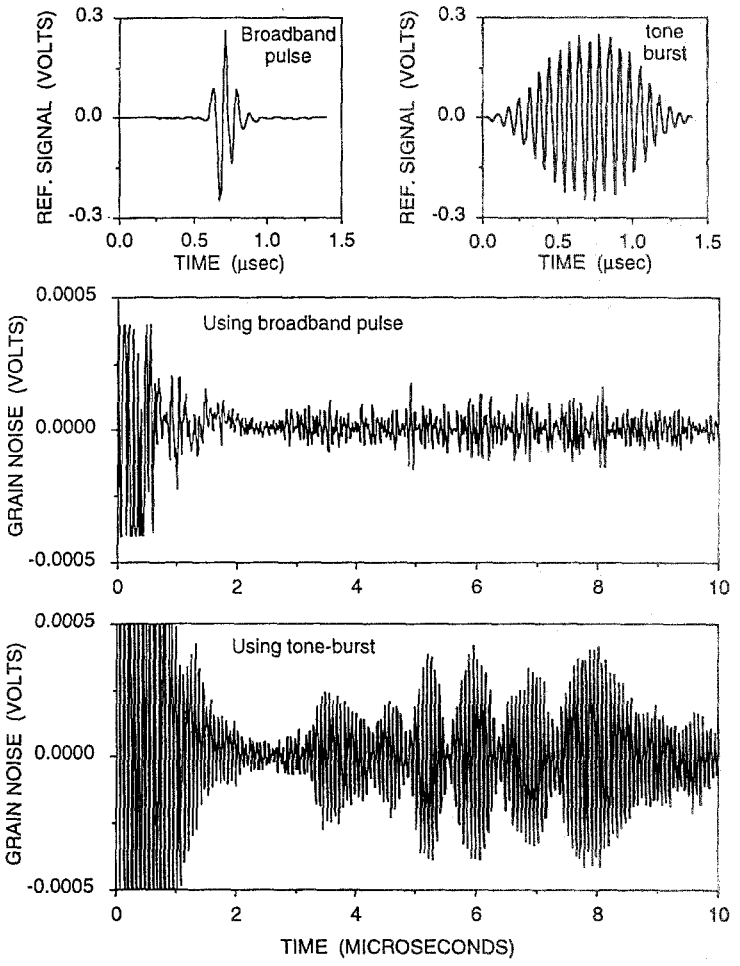

Fig. 2. Front-surface reference signals and backscattered noise signals observed for one position above a titanium specimen. Results are shown for both broadband and toneburst pulses. Specimen TIC side 3; transducer P4 (a=0.607 cm, F=z_{0R}=9.65 cm); z_{0S}=1.0 cm.

The time coordinate is then directly proportional to the depth of beam penetration within the metal specimen.

Typical A-scans showing backscattered noise echoes from a pure titanium specimen are shown in the lower portion of Fig. 2. The two traces were obtained using the same 15-MHz focused transducer positioned at the same point above the specimen. The only difference was the manner in which the transducer was excited: in one case an input toneburst voltage was used, and in the other a voltage spike was input to excite a broadband UT pulse. The corresponding front-surface reference signals are shown in the upper portion of the figure. The two reference signals have approximately the same peak-to-peak amplitudes, but the toneburst pulse carries more energy and leads to considerably more backscattered grain noise. For material characterization studies in low-noise alloys, the higher noise levels seen with toneburst pulses lead to more accurate determination of the material-dependent FOM. As can be seen by comparing the upper and lower panels in Fig. 2, there are generally large differences (50–70 dB) between the amplitudes of the reference and noise signals, necessitating different amplification settings for the two classes of signals. In our subsequent model-based analysis of the noise signals, we assume that the attenuator circuitry behaves linearly over the voltage range in question. We have corrected all measurements for differences in the attenuator settings and presented all results as if the reference and noise signals were acquired at identical equipment settings.

As the transducer in Fig. 1b is scanned, the observed front-surface echo is not noticably altered, but rapid variations in the detailed appearance of the noise signal are seen. However, one can usually observe subtle features common to all noise A-scans which arise from the instrumentation, and are related to the recovery of

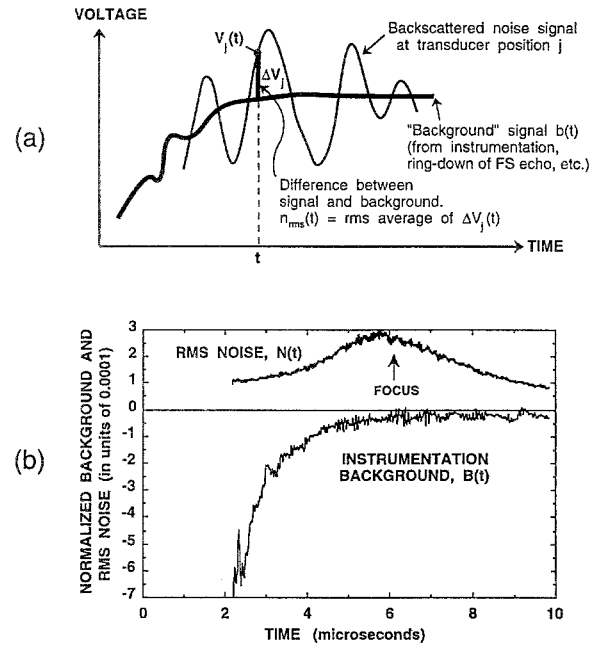

Fig. 3. (a) The meanings of the instrumentation background level $b(t)$ and the average noise level $n_{rms}(t)$. (b) Normalized background level and rms noise level seen in a focused-transducer inspection of a Ti-6246 specimen. (Side 2 of specimen PWL; transducer P4; 15-MHz broadband pulse; z_{0S}=2.0 cm; 500 transducer positions).

linear amplification following the ringdown of the FS echo. By processing many noise signals, one can deduce the instrumentation background level (b) and a measure of the average noise level (n_{rms}) as functions of time. The meaning of these two quantities are illustrated in Fig 3a. $b(t)$ is the time-domain signal which would be seen if no grain scattering had occurred in the specimen, and $n_{rms}(t)$ is defined as the rms positional average of the difference between the observed noise signal and the instrumentation background.

To estimate these quantities in practice, we use[9]

$$b(t)=\frac{1}{M}\sum_{j=1}^{M}V_j(t) \tag{1}$$

and

$$n_{rms}(t) = \left[\frac{1}{M}\sum_{j=1}^{M}(V_j(t)-b(t))^2\right]^{1/2} = \left[\frac{1}{M}\sum_{j=1}^{M}V_j^2(t) - \frac{1}{M^2}\left(\sum_{k=1}^{M}V_k(t)\right)^2\right]^{1/2} \tag{2}$$

where M is the number of transducer positions used, and $V_j(t)$ is the observed voltage at time t for transducer position j. In writing Eq. (1), we are assuming that the effect of grain noise is to cause voltage variations about the instrumentation background level, and that the mean value of these variations is zero when the number of observations (M) is large. Our estimate of the background voltage is then subtracted from each measured voltage when the rms noise level is calculated. Notice that it is not necessary to store the entire waveform for each transducer position in order to compute $b(t)$ and $n_{rms}(t)$. Rather, one need only store the running sums $\Sigma_j V_j(t)$ and $\Sigma_j[V_j(t)]^2$ for each discrete time t at which digitization is performed. To eliminate the dependence of measured noise on equipment gain settings, dimensionless versions of $b(t)$ and $n_{rms}(t)$ are obtained by dividing by E_{max}, defined as one-half of the peak-to-peak amplitude of the reference signal.

$$B(t) = b(t)/E_{max} \quad N_{rms}(t) = n_{rms}(t)/E_{max} \tag{3}$$

We refer to $N_{rms}(t)$ as the "normalized rms noise level" at time t. The noise voltages observed at a given time instant $\{V_j(t); j=1,2,...M\}$ are distributed in a manner which is approximately Gaussian when many grains contribute appreciably to each noise echo. However, when relatively few grains contribute, the distribution can be decidedly non-Gaussian, with more voltages near zero and more voltages at extreme values that would be expected from Gaussian statistics.[15,18] $B(t)$ and $N_{rms}(t)$ may be interpreted as the mean and standard deviation, respectively, of the noise voltage distribution at time t.

Figure 3b displays normalized background and rms noise functions deduced from 500 A-scans observed during examination of a Ti-6246 specimen. Immediately following t=0, there is a time interval during which the trailing portion of the FS echo swamps the grain noise signals; accurate noise measurements are not possible within this interval. The broad maximum of $N_{rms}(t)$ seen in Fig. 3b arises from the focusing of the ultrasonic beam in the metal. The vertical arrow in the figure locates the position of the time-scaled focal point: a metal grain located at the geometrical focus would return an echo that is centered at the indicated time. For effect in Fig. 3b, the instrumentation background signal was allowed to rise slowly toward zero following the FS echo. In practice, the recovery time is substantially reduced by employing a 0.3 MHz or 1.0 MHz high-pass filter when acquiring all reference and noise signals. The usable time interval is bounded by the end of the front-wall echo and the beginning of the first back-wall echo. For focused-probe inspections, it is desirable to have the time-scaled focal point fall within this interval, because the beam models used in subsequent data analysis are most accurate in the focal zone.

The "smoothness" of the deduced $N_{rms}(t)$ function will depend upon the number of spatially-independent noise waveforms used in the averaging process. Figure

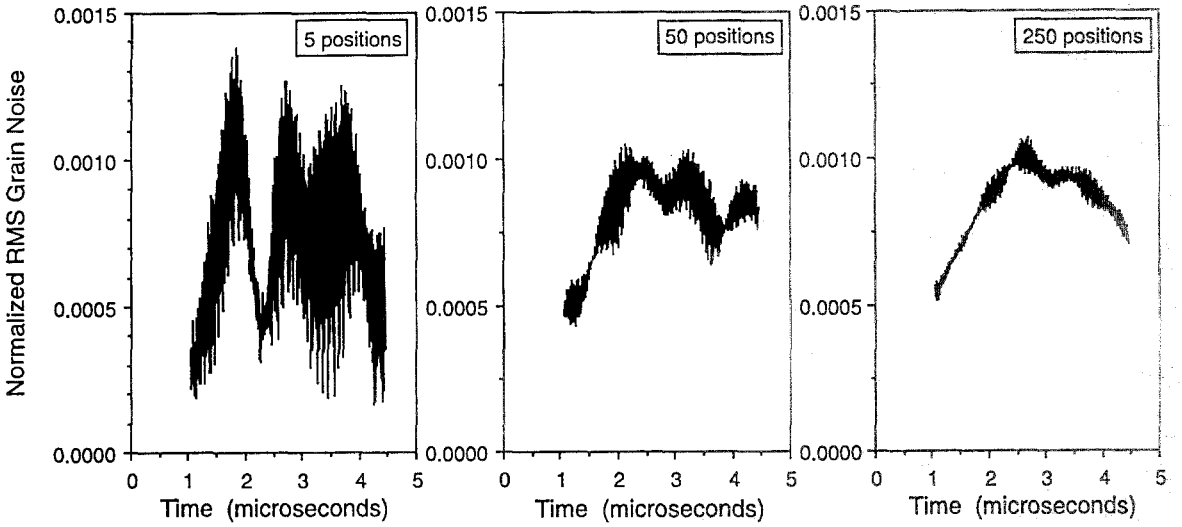

Fig. 4. Deduced rms noise level $N_{rms}(t)$ in an ultrasonic inspection of a titanium specimen, for three choices of the number of transducer positions. (Side 2 of specimen TIC: focused transducer P4; 1-μsec 15-MHz toneburst; z_{0S}=6.0 cm).

4 shows three $N_{rms}(t)$ functions observed during a toneburst inspection of a pure titanium specimen. General progress toward a smooth curve is seen as the number of waveforms increases. We generally used 100–1000 waveforms per analysis, with 500 being a common choice. The corresponding transducer positions were chosen to be as widely spaced as possible, within the constraint that the ultrasonic beam have little interaction with the vertical sides of the specimen. In most cases, the stepsize for transducer motion was smaller than the transducer diameter, but larger than the diameter of the beam in the focal zone. For some of the smaller specimens, noise waveforms at adjacent transducer positions were not completely uncorrelated even in the focal zone. The levelness of the specimen with respect to the scanning directions influences the extracted background level, and hence the deduced rms noise level. For this reason, care was taken to level each specimen to within a fraction of the sound wavelength, by observing the stability of the reference echo during lateral translations of the transducer.

3. MODEL DEVELOPMENT

In the present section we outline the derivation of a model formula which relates the normalized rms noise level to microstructural features of the specimen and to the particulars of the inspection system, assuming the geometry and coordinate system of Fig. 1. A more detailed derivation can be found in Ref. 15. We assume that the observed noise signal is an incoherent sum of echoes backscattered by individual microstructural entities in the metal. These entities may be single metal grains, or collections of grains acting in unison, but they will be referred to simply as "grains" in either case. We assume that the specimen is macroscopically homogeneous, and contains n grains per cubic centimeter. Only single-scattering events are considered explicitly; however, the attenuation of the beam with depth, which can be influenced by multiple scattering, is treated through an effective attenuation constant, α_1. More specifically, we neglect all shear wave components and assume that there is a well-defined, longitudinally-polarized, incident beam propagating through the metal specimen, whose profile is not appreciably "diffused" by grain scattering events. The only assumed effect of grain scattering on the incident beam is to attenuate the beam as it propagates. At a fixed frequency, the beam displacement (or pressure) amplitude at some point a depth z_1 in the metal is written as $U(x_1,y_1,z_1)\exp(-\alpha_1 z_1)$ where $U(x_1,y_1,z_1)$ is the amplitude that would be seen at that point were the metal a nonscattering, non-absorbing medium. We further assume that the beam diameter and wavelength in the metal are large compared to the mean grain size, permitting us to use a specific ultrasonic measurement model[19] to estimate the backscattered signal from a single grain.

Let $R(t)$ denote the observed time-domain front-surface reference echo. (More specifically, $R(t)$ is the time-domain voltage signal appearing in the coaxial cable of the transducer that is generated when the front surface echo returns to the transducer). Using the same time origin and pulser settings, let $\delta S(t,x_1,y_1,z_1)$ similarly denote

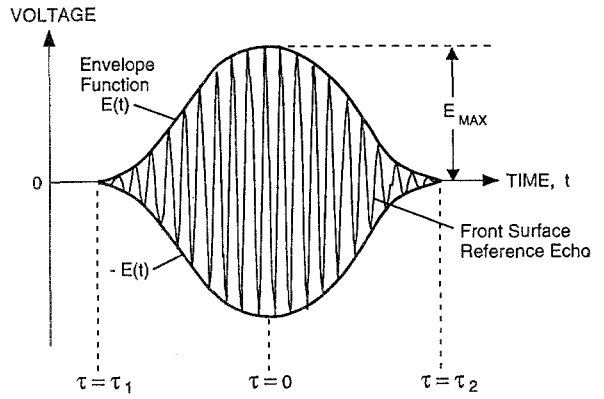

Fig. 5. The envelope function $E(t)$ of the front surface reference signal. The time coordinate τ plays the role of an integration variable in the model.

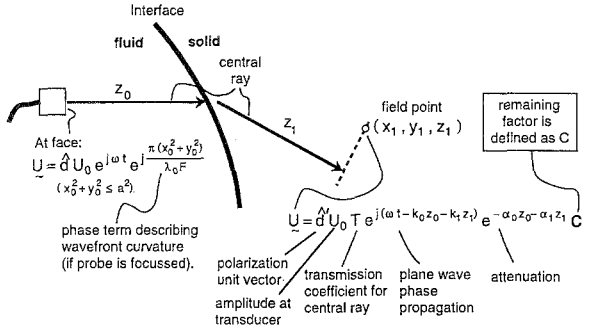

Fig. 6. $C(x_1,y_1,z_1)$ is a dimensionless measure of the ultrasonic displacement field.

the voltage signal that would be observed in the noise-measurement geometry due to scattering of the incident sound pulse by a single metal grain located at position (x_1,y_1,z_1). We assume that the observed reference signal is a narrow-band toneburst of angular frequency ω_0, which can be approximated as $R(t)=E(t)\cos(\omega_0 t+\phi)$. As illustrated in Fig. 5, $E(t)$ is a slowly varying envelope function which is non-zero only over a finite time range. Our final model expressions will be independent of the value of the phase ϕ, and we now set $\phi=0$ to simplify the presentation. In addition, we adopt the usual convention whereby real-valued quantities such as voltage or displacement are written in complex form, with the understanding that the physical value is the real part of its complex counterpart. Thus the reference signal voltage is written as

$$R(t) = E(t)e^{j\omega_0 t} \tag{4}$$

The Fourier transforms of $R(t)$ and $\delta S\ (t,x_1,\ y_1,\ z_1)$ will be denoted by $\Gamma_{ref}(\omega)$ and $\delta\Gamma_s(\omega,\ x_1,\ y_1,\ z_1)$ respectively:

$$R(t) = \int_{-\infty}^{\infty} \Gamma_{ref}(\omega)e^{j\omega t}d\omega \tag{5}$$

$$\delta S(t,x_1,y_1,z_1) = \int_{-\infty}^{\infty} \delta\Gamma_s(\omega,\ x_1,y_1,z_1)e^{j\omega t}d\omega \tag{6}$$

The measurement model of Thompson and Gray[19] can be applied to obtain approximate expressions for Γ_{ref} and $\delta\Gamma_s$. That model uses Auld's electromechanical reciprocity relationship[20] to relate electromagnetic fields in the transducer's coaxial cable to sonic fields in the liquid and solid media. In addition, the model invokes paraxial beam approximations, and assumes that the incident sonic field can be approximated by a plane wave over the dimensions of a (small) scatterer. In our application of the measurement model, the grain in question is treated as an isolated scatterer located in the homogeneous "average" medium formed by the other grains in the specimen. James Rose[21,22] demonstrates that when the homogeneous medium is defined as the Voigt average over the grains, then the single-scattering approach which we adopt leads to the first term in Rose's systematic expansion for the backscattered noise. From Ref. 19 we have

$$\Gamma_{ref}(\omega) = \beta(\omega)R_{00}D(\omega)\exp(-2jk_0z_{0R}-2\alpha_0z_{0R}) \tag{7}$$

$$\delta\Gamma_S(\omega,x_1,y_1,z_1) = \left[\frac{2\beta(\omega)A(\omega,x_1,y_1,z_1)\rho_1 v_1}{jk_1a^2\rho_0 v_0}\right]T_{01}^2C^2(\omega,x_1,y_1,z_1) \cdot\exp\left[-2j(k_0z_{0S}+k_1z_1)-2\alpha_0z_{0S}-2\alpha_1z_1\right] \tag{8}$$

In these expressions v, k, ρ, α, and a denote longitudinal wave velocity, wavevector ($k=\omega/v$), density, attenuation constant, and transducer radius, respectively. $A(\omega,x_1,y_1,z_1)$ is the scattering amplitude for longitudinal backscattered sound from the grain in question. $\beta(\omega)$ is a transducer efficiency factor, suitably scaled so that Γ_{ref} and $\delta\Gamma_s$ may be directly interpreted as voltage spectral components. R_{00} and T_{01} are reflection and transmission coefficients at the water/metal interface for plane wave displacement fields propagating in the central ray direction (i.e., along the z axis). $C(\omega,x_1,y_1,z_1)$ is a measure of the incident ultrasonic displacement field in the metal when the transducer face oscillates harmonically at angular frequency ω. As illustrated in Fig. 6, the harmonic displacement field is written as a product of factors, with term C essentially describing the effects of focusing, refraction, and diffraction. $D(\omega)$ accounts for the effects of diffraction losses in the reference signal, and, for a planar transducer, is unity in the absence of diffraction

(high frequency limit). More specifically, if the velocity at each point on the (possibly curved) face of the transducer is $V_0 \exp(j\omega t)$, then $D(\omega)$ is defined as the integral of the reflected velocity field over the area of the transducer face, divided by $\pi a^2 V_0 R_{00} \exp(j\omega t - 2jk_0 z_{0R} - 2\alpha_0 z_{0R})$. In addition to the explicitly noted dependence on frequency, C and D also depend upon transducer characteristics (a and F), waterpaths, and speeds of sound.

To obtain an approximate expression for δS, the time-domain echo from the grain, we begin by solving Eq. (7) for β and substituting the result into Eq. (8). The new expression for $\delta\Gamma_s$ is then inserted into the right-hand side of Eq. (6). The resulting integral contains $\Gamma_{ref}(\omega)$ which is sharply peaked near $\omega=\omega_0$. All constants and slowly varying functions in the integrand (i.e., all factors except $\Gamma_{ref}(\omega)$ and the complex phase terms) are collected into a term H, evaluated at $\omega=\omega_0$, and factored outside of the integral. Using Eq. (5) and $k=\omega/v$, the remaining integral is recognized as $R(t-t_0)$ where

$$t_0 = 2\frac{(z_{0S}-z_{0R})}{v_0} + \frac{2z_1}{v_1} \tag{9}$$

represents the time delay between the reference and grain-scattered signals. The result for δS is

$$\delta S(t,x_1,y_1,z_1) = H(\omega_0,x_1,y_1,z_1)E(t-t_0)e^{j\omega_0(t-t_0)} \tag{10}$$

where

$$H(\omega_0,x_1,y_1,z_1) = \frac{2T_{01}^2 A(\omega_0,x_1,y_1,z_1)\rho_1 v_1}{R_{00}D(\omega_0)jk_1 a^2 \rho_0 v_0} C^2(\omega_0,x_1,y_1,z_1) \exp[2\alpha_0(z_{0R}-z_{0S})-2\alpha_1 z_1] \tag{11}$$

In Eq. (11) it is understood that α_0 and α_1 are evaluated at $\omega=\omega_0$. Comparing Eqs. (4) and (11) the backscattered signal from the grain is seen to be a time-shifted copy of the reference signal with the overall amplitude and phase modified by the complex factor H.

The normalized rms noise level, as defined in Section 2, is the square root of the average square of the measured noise voltage, divided by the peak amplitude of the reference signal. Assuming the instrumentation background level to be zero at all times (so that $\Delta V_j = V_j$ in Fig. 3a), this may be expressed as

$$N_{rms}(t) = \frac{\sqrt{<[\mathrm{Re}(V_j(t))]^2>}}{E_{max}} \tag{12}$$

where $< >$ denotes the average over many independent ensembles of grains, and the ensembles are enumerated using index j. We now assume that the noise voltage $V_j(t)$ arises from the superposition of directly-backscattered signals from all insonified grains in ensemble j, and the index i is introduced to enumerate those grains:

$$\mathrm{Re}[V_j(t)] = \sum_{i=1}^{m} \mathrm{Re}[\delta S_i] = \sum_{i=1}^{m} |B_i|\cos(\omega_0 t+\phi_i) \tag{13a}$$

where

$$|B_i| = |H_i(\omega_0,x_{1i},y_{1i},z_{1i})E(t-t_{0i})|$$

and

$$\phi_i = -\omega_0 t_{0i} + \text{phase of } H_i \tag{13b}$$

In the ensemble average of the square of Eq. (13a), the amplitude and cosine factors are effectively independent. $|B_i|$ is a slowly varying function of position through the attenuation and diffraction/focusing in Eq. (11), while ϕ_i is a rapidly-varying function of depth through the $-\omega_0 t_{0i}$ term in Eq. (13b). In addition, ϕ_i depends on the phase of the scattering amplitude for grain i, which will vary randomly from ensemble to ensemble. Moreover, the phases of two grains in the same ensemble are expected to be unrelated, even if they are closely spaced, since the two grains will have different principal axes orientations and hence different impedance mismatches with the assumed Voigt averaged medium. Accordingly, we now impose our assumption of incoherency, i.e., that the phases of the signals resulting from distinct grains are, on average, independent of one another. In that event,

$$<[\mathrm{Re}(V_j(t))]^2> = \sum_{i=1}^{m}\sum_{k=1}^{m} <|B_i||B_k|><\cos(\omega_0 t+\phi_i)\cos(\omega_0 t+\phi_k)> = \frac{1}{2}\sum_{i=1}^{m} <|B_i|^2> \tag{14}$$

where the ensemble average of the product of cosines has been performed by writing the product as $[\cos(\phi_i-\phi_k)+\cos(2\omega_0 t+\phi_i+\phi_k)]/2$ and averaging over all possible values of $(\phi_i-\phi_k)$ and $(\phi_i+\phi_k)$ when $i\neq k$. The only factor now affected by the ensemble-averaging operation is the magnitude of the single-grain scattering amplitude $|A_i|$.

To complete the derivation, we now replace the sum over grains in Eq. (14) by an integral over the volume of the metal, introducing n as the number of grains per unit volume. This is appropriate whenever the number of grains in the region defined by the beam width and the spatial length of the reference pulse in the solid is large. Assuming that the specimen is homogeneous, and hence that average microstructural properties are independent of position, the ensemble average of the

square of the scattering amplitude may be factored from the integral. The final result for the normalized rms noise level is

$$N_{rms}(t)=\text{FOM}\cdot\left|\frac{\sqrt{2}T_{01}^2\rho_1 v_1\exp(-2\alpha_0(z_{0S}-z_{0R}))}{R_{00}a^2\rho_0 v_0 D(\omega_0)k_1}\right|$$

$$\left[\int_0^\infty G(z_1)\left|\frac{E(t-t_0)}{E_{max}}\right|^2\exp(-4\alpha_1 z_1)dz_1\right]^{1/2} \quad (15)$$

where

$$G(z_1)=\int_{-\infty}^{\infty}\int_{-\infty}^{\infty}|C(\omega_0,x_1,y_1,z_1)|^4 dx_1 dy_1 \quad (16)$$

and where the microstructural Figure-of-Merit is defined as the product of the square root of the density of grains and the rms averaged single-grain backscatter amplitude at the toneburst frequency,

$$\text{FOM}=\sqrt{n}A_{rms}=\sqrt{n}<|A(\omega_0)|^2>^{1/2} \quad (17)$$

The square of the FOM is often termed a "backscatter coefficient" by other authors, e.g., Refs. 6 and 11. When discussing the contribution of microstructure to the backscattered grain noise, we prefer to use the FOM rather than the more common backscatter coefficient. This is because our primary emphasis is on backscattered noise voltage, as observed in conventional ultrasonic A-scans, and the noise voltage level is directly proportional to the FOM.

In addition to the FOM factor, the effects of grain scattering also enter our calculation through the attenuation factor $\exp(-4\alpha_1 z_1)$ appearing in the integral over z_1. Presumably, $\alpha_1(\omega_0)$ is a function of n and $A_{rms}(\omega_0)$; however, no effort is made in this work to explicitly incorporate that function. The term $G(z_1)$ is associated with the scattering from a thin layer of grains at depth z_1; the integration over z_1, which is weighted by the toneburst envelope function ensures that all grains contribute to the noise signal at time t except those forbidden by time-of-flight considerations.

The choice of time origin in Eqs. (4)–(15) is arbitrary. In experiments, we generally define $t=0$ to be the center time of the FS echo (i.e.., midpoint of the interval over which echo envelope exceeds 20% of its peak value) seen when the waterpath is z_{0S}. At our level of approximation, this is equivalent to choosing $t=0$ at the center of an echo from a single grain located on the water/metal interface. Making this choice, the integral over z_1 in Eq. (15) may be expressed as

$$\int_0^\infty G(z_1)\left|\frac{E(t-t_0)}{E_{max}}\right|^2\exp(-4\alpha_1 z_1)dz_1=\frac{v_1}{2}$$
$$\int_{\tau_1}^{\tau_2} G(z_1)\left|\frac{E(\tau)}{E_{max}}\right|^2\exp(-4\alpha_1 z_1)d\tau \text{ with } z_1=\frac{v_1}{2}(t-\tau) \quad (18)$$

Here, as illustrated in Fig. 5, the integration variable is a time coordinate (τ) which is defined to be zero at the center of the FS reference signal; the envelope function of the reference signal is non-zero on $\tau_1\le\tau\le\tau_2$. The manner in which the duration of the reference signal and time-of-flight consideration combine to limit the depths of contributing grains is now manifest in Eq. (18).

Our model expression for $N_{rms}(t)$, Eqs. (15)–(18), can be used in two distinct ways. If the specimen FOM is known *a priori*, then Eq. (15) can be used to predict the rms noise level for any assumed inspection scenario with the geometry of Fig. 1. (In making such predictions, the FS reference signal, transducer characteristics, waterpaths, wavespeeds, densities, and attenuations are assumed to be known). Alternatively, Eq. (15) may be solved for the FOM, and thus the FOM can be evaluated if $N_{rms}(t)$ has been measured at any single time instant. We refer to this latter use as the model-based "extraction" of the FOM from measured noise data. When a specimen with undocumented or complex microstructure is received for study, the most practical way of obtaining the FOM is by extraction from noise data. In such a case, the FOM is effectively being defined, through Eq. (15) above, as a simple measure of the normalized noise after separation of the measurement system effects. Such a generalized definition is useful so long as the extracted FOM proves to be independent of the measurement system used. For single-phase microstructures and experimental circumstances where multiple-scattering effects are not appreciable, the generalized FOM is expected to equal $\sqrt{n}A_{rms}$.

For either use of the model, the terms R_{00}, T_{01}, E, D, and C must be evaluated. the normal-incidence plane-wave reflection and transmission coefficients are well known, and are given by

$$R_{00}=\frac{\rho_0 v_0-\rho_1 v_1}{\rho_0 v_0+\rho_1 v_1} \quad T_{01}=\frac{2\rho_0 v_0}{\rho_0 v_0+\rho_1 v_1} \quad (19)$$

The envelope function of a measured reference signal, $E(t)$, can be obtained in two ways. Since the sampling rate is generally large compared to the toneburst frequency, an upper envelope function can be obtained by fitting a spline curve through the positive peak points of the reference signal. A similar lower curve can be ob-

tained using the negative peaks, and the magnitudes of the two curves can be averaged to obtain $E(t)$. Alternatively, $E(t)$ may be determined using Fourier analysis methods, after the fashion of Ref. 23. When evaluating time-harmonic field quantities, we assume that the transducer functions as an ideal piston probe, having a circular piezoelectric element of radius a, and, possibly, having a spherical lens with a geometric (ray limit) focal length F in water. For the planar transducer case, an expression for the reference signal diffraction correction is given in Ref. 24:

$$D(\omega) = 1-e^{-2\pi j/S}\left[J_0\left(\frac{2\pi}{S}\right) + jJ_1\left(\frac{2\pi}{S}\right)\right]; \; S = \frac{4\pi v_0 z_{0R}}{\omega a^2} \quad (20)$$

Here J_m denotes the ordinary Bessel function of integer order m,[25] and the waterpath z_{0R} is arbitrary. The same expression may be used to evaluate D for a focused piston transducer if the waterpath is equal to the geometrical focal length ($z_{0R}=F$ only), as is our measurement practice. In that case, the diffraction correction for the focused transducer equals the negative of the complex conjugate of the expression on the right-hand side of Eq. (20).[26]

For results presented in the ensuing sections, either a Gaussian or Gauss-Hermite beam model is used to evaluate the diffraction/focusing factor C and its integral G. In the first approach, we imagine replacing the piston transducer element by one which oscillates with a Gaussian amplitude profile. The amplitude of oscillation at the center of the face, and the rate of decrease with radial distance are chosen such that the radiated field of the Gaussian transducer approximates the central lobe of the radiation pattern of the piston transducer in the focal zone or far field. In particular, Eqs. (38)–(39) of Ref. 27 are used to relate the parameters of the piston and Gaussian transducers, Eqs. (10)–(15) of that reference are assumed to describe the z-component of the displacement field propagating in the water or metal, and Eq. (32) is used to connect the two fields across the interface. When the Gaussian beam model is used, the integrations over x_1 and y_1 in Eq. (16) can be performed analytically, with the result

$$G(z_1) = 4.356a^2\frac{1+\delta^2}{\left[\left(\frac{z}{F}\right)(1+\delta^2)-1\right]^2+\delta^2} \quad (21)$$

where

$$z = z_{0S}+\frac{v_1}{v_0}z_1 \qquad \delta = 3.539\frac{v_0 F}{\omega_0 a^2} \quad (22)$$

For more accurate evaluations of G, the Gauss-Hermite beam model[28] is used, as described in detail in Ref. 15. Briefly, we assume that the displacement field on the facial ($z_0=0$) plane of the transducer has the form specified in Fig. 6. This known initial field is expanded in a truncated set of Gauss-Hermite (GH) basis functions, which are solutions to the wave equation under a paraxial (Fresnel) approximation. Each basis function is propagated through the water or metal medium using the wave equation, and through the interface using paraxial rules based on Snell's Law. The basis functions are then evaluated and summed to determine the displacement field at a given point in the metal. Regarded as a function of the lateral coordinates x and y, the form of each basis function is preserved during propagation through space or transmission through an interface. However, changes occur in the values of certain parameters which describe the overall amplitude, lateral width, radius or phase curvature, and excess propagation phase. The application of the GH model is principally a bookkeeping exercise in which one tracks the values of these parameters for each basis function from the transducer to the evaluation point. When calculating the displacement field or, equivalently, C, we have retained all basis functions having Hermite polynomial order ≤ 30 in x or y. The integrations required to calculate $G(z_1)$ when then performed numerically.

4. DEPTH DEPENDENCE OF BACKSCATTERED NOISE

In Eq. (15), the time dependence of the backscattered noise is primarily determined by the beam integral $G(z_1)$ which describes the contribution of the incident radiation pattern to the scattering from a plane of grains at depth z_1. Note that when the metal attenuation (α_1) and envelope duration ($\tau_2-\tau_1$) are small, $N_{rms}(t)$ is approximately proportional to $\sqrt{G(z_1=t/2v_1)}$, which may be interpreted as a "diffraction correction" in the noise model. The physical reason for the peaking of N_{rms} near the beam focal point now becomes clear. In the absence of attenuation, conservation of energy implies that a beam of lateral width $w(z_1)$ will have amplitude $C\propto 1/w(z_1)$. As the beam narrows, the number of insonified grains [$\propto w^2(z_1)$] drops but the backscattered power from each such grain [$\propto C^4 \propto 1/w^4(z_1)$] increases. The sum of the backscattered powers from the insonified grains is

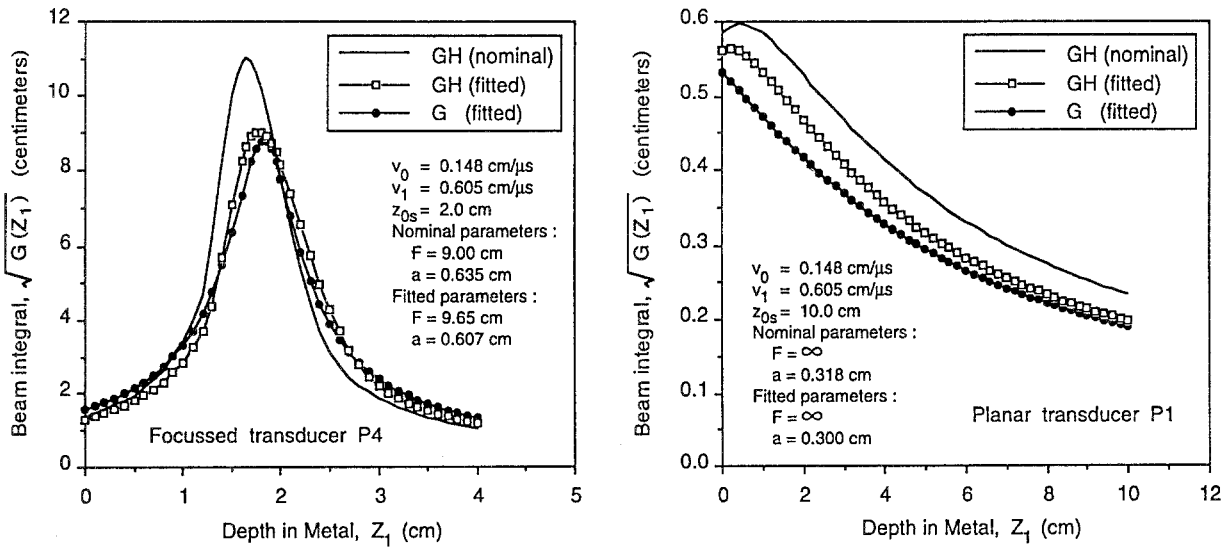

Fig. 7. Square root of the beam integral as a function of depth for two cases of interest. Results are displayed for GH beam model calculations using the nominal (—) and fitted (-□-) transducer parameters and for a Gaussian beam calculation using the fitted parameters (-●-). The longitudinal wavespeed on the metal is that of Ti-6246 specimen PWL, and the frequency is 15 MHz.

then proportional to $1/w^2(z_1)$, and the rms noise level to $\sqrt{G(z_1)} \propto 1/w(z_1)$. Hence regions in which the beam has the narrowest width will produce the greatest noise level.

We use the notation *Pi*, i=1,2,3,... to identify the various transducers used in our experiments. (The radii and focal lengths for five of the transducers are later listed in Panel (a) of Fig. 11.) In Fig. 7, we display $\sqrt{G(z_1)}$ at 15-MHz for two inspections of a titanium alloy, one using a focused transducer (P4), and one using a planar transducer (P1). In each case three calculations were performed, using different approximations for the radiation pattern of the transducer. The first calculation employed the GH beam model and assumed the nominal values for radius (a) and focal length (F) quoted by the transducer manufacturer. The second calculation also employed the GH beam model, but assumed a and F values determined by a transducer characterization procedure[15,16] in which the 3D radiation pattern in water is mapped (by measuring the echoes from a small reflecting sphere), and the (a, F) parameters in the GH model are then adjusted to achieve the best agreement between the measured and model fields at the inspection frequency. The third calculation assumed the fitted values of a and F but used the simpler Gaussian beam model. For the focused case $\sqrt{G(z_1)}$ is observed to possess a pronounced maximum near to, but slightly in front of, the geometric focus. (The geometric focal point is located at a metal depth of 1.71 cm for the nominal focused piston transducer, and at 1.87 cm for the fitted one.) For the planar case the far-field parameter [$S = 2\lambda_0 z_0/a^2$] is greater than unity for round trip travel to the water/metal interface, and $\sqrt{G(z_1)}$ is observed to decrease slowly with depth, due to the steady divergence of the beam as it propagates through the metal. For our paraxial beam models, the only property of the metal which influences the value of $G(z_1)$ is the longitudinal wave speed v_1.

For both the planar and focused cases in Fig. 7, the different treatments of the transducer lead to noticeably different results for $\sqrt{G(z_1)}$. In each case, the difference between the two GH calculations (one using nominal and one using fitted transducer properties) is larger than the difference between the two calculations using fitted properties (one using the GH model and one using the Gaussian model). Thus the error resulting from using the simpler beam model is smaller than the error arising from imperfect knowledge of the transducer. These examples indicate that it makes little sense to proceed with the computationally-intensive GH model calculation unless the transducer has been accurately characterized.

5. TESTS OF THE MODEL USING SYNTHETIC NOISE SIGNALS

If the Figure-of-Merit of the specimen is known, a straightforward direct test of the noise model is possible. Using some particular transducer and input toneburst ex-

citation, one simply measures the normalized rms noise level as a function of time, and compares with that predicted by Eq. (15). Unfortunately, the FOM of a specimen under study is generally not known *a priori*, and less direct methods are required to test the model. Before discussing these we will report on a series of direct tests usign synthetic noise signals calculated by a Monte Carlo method (MCM). The MCM procedure is described in detail in Refs. 15 and 18. Briefly, one assumes a particular grain density, and fills a metal volume with an appropriate number of spherical single-crystal grains. Random number generators are used to determine the precise location, size, and crystallographic orientation of each grain. From these attributes, the scattering amplitude $A(\omega)$ of the grain can be calculated using the Born approximation, which applies because the scattering is weak. One also assumes a particular inspection geometry, as well as a particular front-surface reference echo. From the known reference signal, the spectral components of the echo from each grain can be calculated using Eqs. (7) and (8), and the time-domain echo can then be obtained by an inverse Fourier transform. The echoes from all grains are then summed to obtain the total noise signal. This procedure is repeated for many ensembles of grains, and the resulting collection of synthetic noise signals can then be analyzed using Eqs. (1) and (2) to determine the normalized rms noise level as a function of time.

For such model specimens composed of spherical grains, the distribution functions governing grain sizes and scattering amplitudes are known. Consequently, the FOM of the model specimen may be calculated directly from Eq. (17). With the FOM thus determined, the toneburst noise model can be used to calculate the rms noise level as a function of time (Eq. 15) and this can then be compared to the rms noise level function obtained from the synthetic noise waveforms.

For the study at hand we postulated: (1) an isotropic specimen of equi-axed α-phase (hexagonal) titanium containing n grains per cubic centimeter, with n ranging from 100 to 100,000 cm^{-3}, (2) insonification using focused transducer P4 (a=0.607 cm, F=9.65 cm), (3) a 15-MHz toneburst of approximately 1-μsec duration, (4) negligible solid attenuation (α_1=0), and (5) 500 ensembles of grains for each choice of n. In Fig. 8, we display the assumed FS reference signal and three typical synthetic total noise signals for the case n=100,000. Because only a portion of the metal volume is filled by model grains, these MCM signals are only valid within the time interval bounded by the arrows (approximately 2 μs≤t≤4μs). For each choice of grain density, the normalized rms noise level of the collection of 500 synthetic noise signals is displayed as a function of time in Fig. 9, and compared with the predicted $N_{rms}(t)$ calculated from Eq. (15) using the known FOM, transducer characteristics, and reference signal. The overall agreement is excellent. Presumably, if the number of ensembles considered in the MCM calculations were increased, the resulting $N_{rms}(t)$ curves would become smoother and better resemble their model counterparts. Notice in Fig. 9 that the average noise level increases with the grain density. This trend holds for the densities listed in the figure, but reverses at higher densities when the Rayleigh regime is approached.[15] In summary of that discussion, note that it is clear that the noise must vanish when $n \to 0$ (single crystal limit) or $n \to \infty$ (infinitesimal grains), and hence the noise must peak at intermediate n.

In the test presented here, the toneburst noise model and MCM share a number of common elements. Both make use of measurement model formulas for expressing the spectral components of the reference signal and the single-grain echoes, and both use the Gaussian beam model for displacement field calculations, and both neglect multiple scattering effects. Thus the comparison in Fig. 9 is principally a test of the approximations which lead from Eqs. (7) and (8) to Eq. (15), and of the incoherent superposition assumption, neither of which are required by the MCM.

In principle, for these model comparisons, it would have been preferable to use higher grain densities to insure that each grain was small compared to a sound wavelength. That would insure that the "small scatterer" assumption of the Thompson–Gray measurement model was satisfied, i.e., that the incident pressure field was essentially constant over the volume of each scatterer. Unfortunately, it was not practical to carry out repeated Monte-Carlo calculations with ensembles containing more than a few hundred thousands grains. Even though the small-scatterer assumption did not always hold, it was violated in the same manner in both the MCM and the toneburst noise model calculations. Each effectively used only the incident pressure amplitude at the center of a scatterer to calculated the scattered response. Thus our test of the incoherent superposition principle and the other approximation leading to Eq. (15) remains valid.

6. TESTS OF THE MODEL USING MEASURED NOISE SIGNALS

In any material, one can test the toneburst noise model to within an overall scale factor by using Eq. (15)

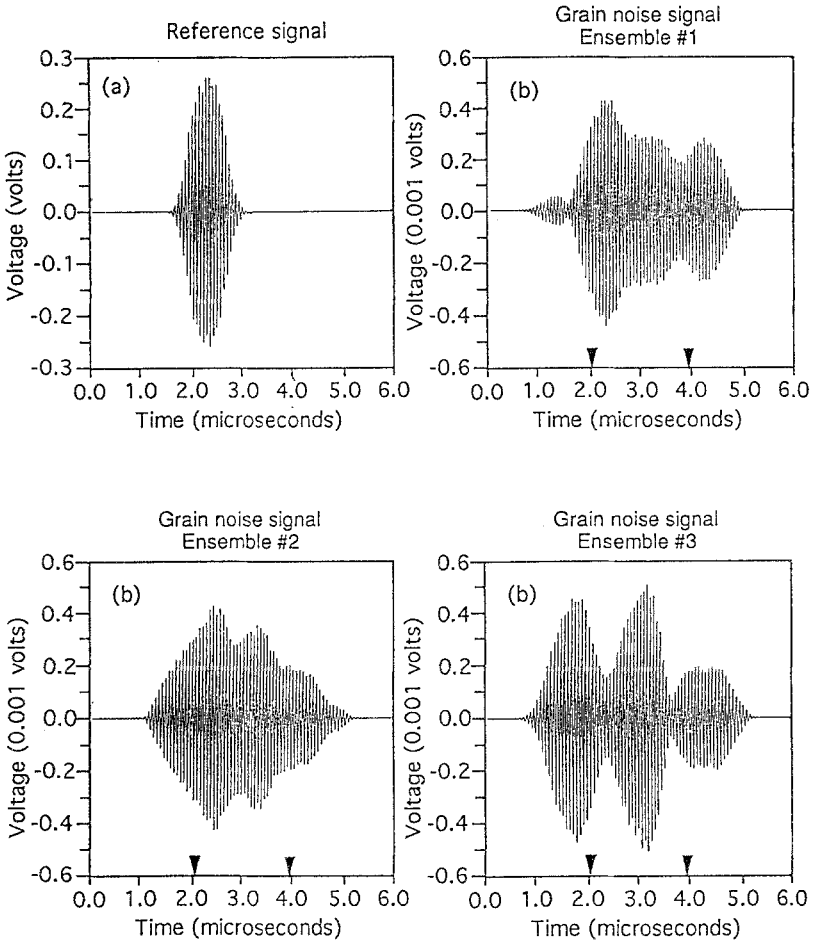

Fig. 8. (a) Front-surface reference echo assumed for MCM calculations of backscattered noise in α-titanium, (b) calculated total noise signals for three ensembles of grains when n=100000 grains/cm^3.

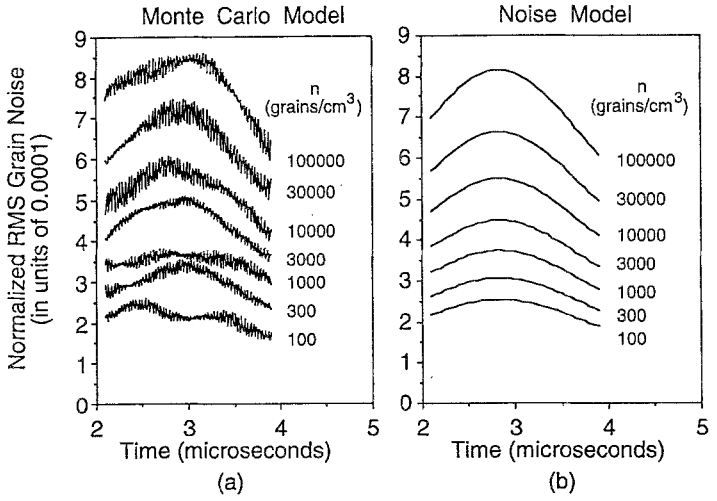

Fig. 9. Normalized rms noise level in model specimens of α-phase pure titanium, as calculated by: (a) the Monte-Carlo method (500 ensembles), (b) the toneburst noise model of Eq. (15). (Transducer P4; 1-μsec, 15-MHz toneburst; z_{0S}=6.0 cm).

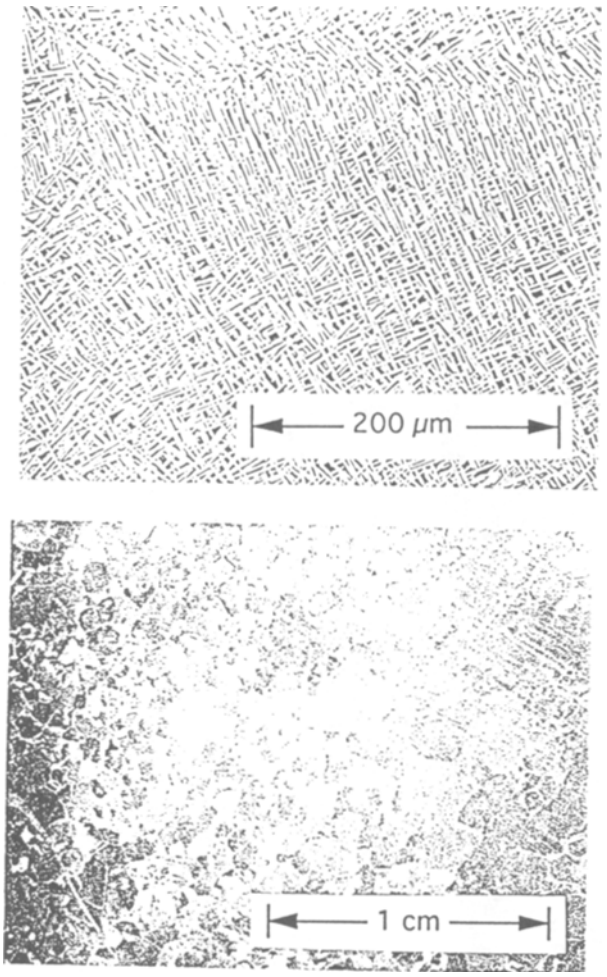

Fig. 10. Optical photographs revealing the microstructure (top) and macrostructure (bottom) of Ti-6246 specimen PWL, side 1.

to "extract" the FOM of the specimen from the measured $N(t)$ value. Such an extraction can be performed anew at every time instant for which $N(t)$ was measured, and, ideally, the resulting FOM values should be independent of time. Moreover, if the toneburst frequency is fixed, the same extracted FOM value should result from experiments using different transducers, or tonebursts of different duration. In the present section we test the model in this manner using noise data from a representative specimen of Ti-6246 designated PWL.[10,15] This specimen had dimensions of 6.0 cm×6.3 cm×10.7 cm, a density of 4.64 gm/cm^3, and longitudinal wavespeeds of 0.605, 0.609, and 0.607 cm/μs for propagation perpendicular to sides 1, 2, and 3, respectively. Photographs of side 1, after polishing and etching, are displayed in Fig. 10. Notice that the specimen possesses structure on two length scales. On a coarse scale, as shown in the lower photograph, irregularly shaped regions with dimensions of a few millimeters are seen. These are thought to be prior beta grains (PBGs), i.e., regions which were beta-phase (cubic) single crystals at an early, high-temperature state in the processing history. Within these regions are much smaller alpha (hexagonal) and beta grains, the former having a needle-like appearance with diameters of a few microns and lengths on the order of 100 microns. X-ray diffraction studies on similar specimens[29] suggest that there is partial alignment of crystalline axes for grains within a given PBG. Photographs of the fine microstructure taken on three orthogonal faces of the specimen appear very similar to one another. However, noticeable differences can be seen when the larger "macrostructural" elements are viewed from the three orthogonal directions. Roughly speaking, the PBGs appear to be pancake-shaped objects which are generally aligned with one another, but not quite aligned with the physical sides of the specimen. Specimen side 1 (or side 4) is most nearly parallel to the large flattened sides of the pancakes, and measured noise levels are several times larger for insonification through sides 1 and 4 than for the other four sides.

In principle, for a weakly-scattering homogeneous material, the FOM deduced from backscattered noise should be independent of the transducer used in the measurement. To test the invariance in practice, a series of noise measurements was made through side 1 of specimen PWL, with the results summarized in Fig. 11. Five 15-MHz transducers, designated P1 through P5, were employed; three focused and two planar. The waterpaths used and the transducer characteristics assumed in the ensuing model calculations are listed in panel a of the figure. For each transducer, the MATEC pulser was adjusted so that the FS reference echo was a 15-MHz toneburst of approximately 1-μsec duration. Envelope shapes for the five transducers were not identical, but generally resembled that of the reference signal shown in Fig. 8a. Backscattered noise signals were acquired at 500 positions for each transducer and analyzed using Eqs. (1) and (2) to determine the normalized rms noise level, $N_{rms}(t)$. Results are shown in panel b of Fig. 11.

The $N_{rms}(t)$ curve of each focused transducer displays the customary prominent maximum centered near the round-trip travel time to the focal zone [$t=2(F-z_{0S})$ v_0/v_1^2]. The $N_{rms}(t)$ curve of each planar transducer, in contrast, is relatively flat and drops slowly in time. The effect of defocussing the beam, by proceeding from a focused transducer (e.g., P5) to a narrow diameter planar transducer (P1) to a large diameter planar transducer (P2) is seen to decrease the normalized noise level. Roughly speaking, the normalized rms noise level is in-

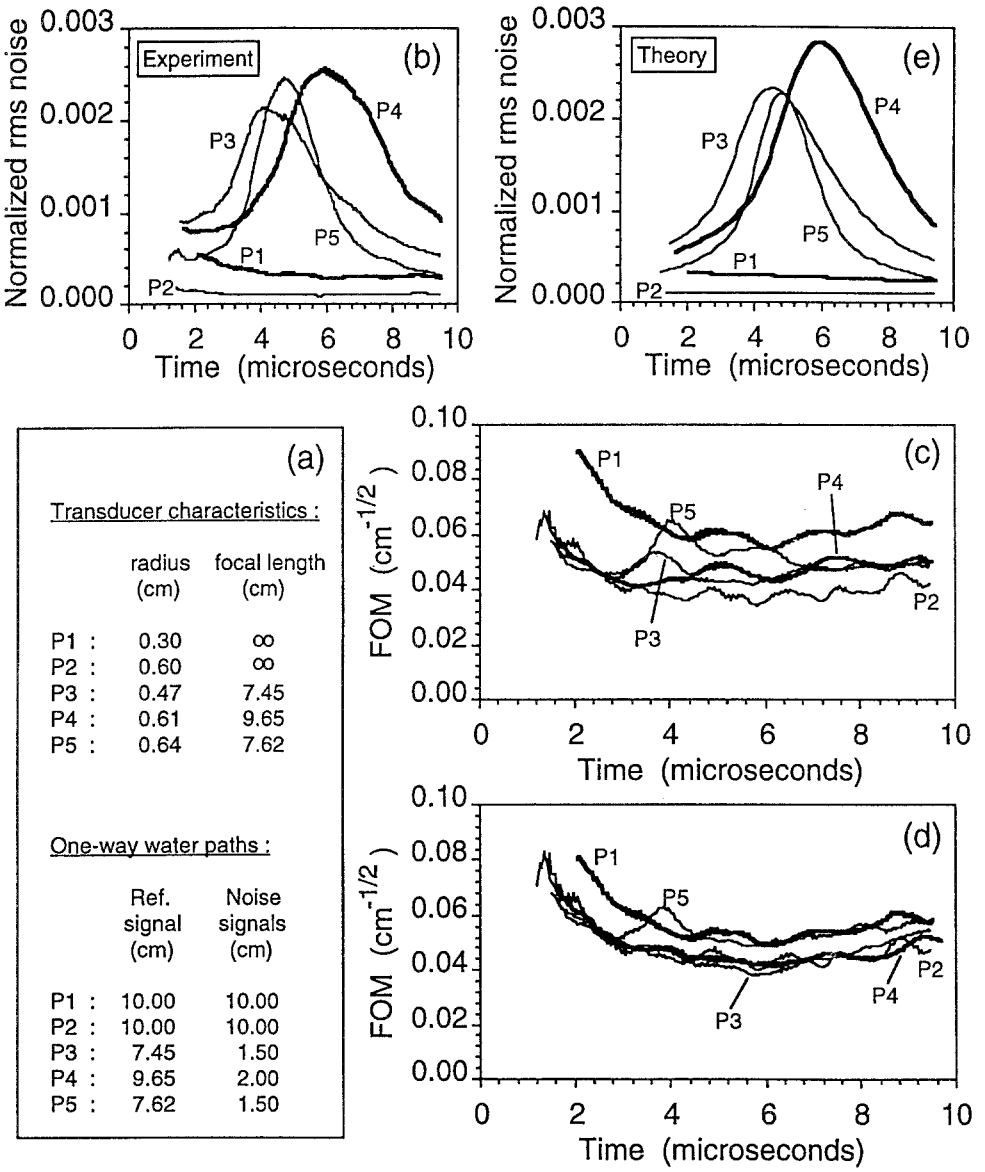

Fig. 11. Effect of transducer choice on backscattered noise: specimen PWL side 1; 15-MHz, 1-μsec tonebursts; 500 transducer positions. (a) Transducers and waterpaths used in five successive experimental trials. The effective radius (*a*) and geometric focal length (*F*) are listed. (b) Measured normalized rms noise level for each trial (5-point smoothing). (c) and (d) FOM at 15-MHz extracted from noise data using Eq. (15) and the Gaussian (*c*) or Gauss-Hermite (*d*) beam model ($\alpha_1=0$). (e) Predicted normalized rms noise levels for the five trials using Eq. (15) with the GH beam model and FOM=0.048cm$^{-1/2}$.

versely proportional to the beam diameter, as discussed earlier.

For each transducer, Eq. (15) was used to extract the FOM from the measured $N_{rms}(t)$ values. The extraction calculations were performed twice, using the Gaussian and Gauss-Hermite beam models in turn. In all calculations the attenuation coefficient for specimen PWL was assumed to be negligible ($\alpha_1=0$) for reasons which will be discussed in Section 7. The five resulting FOM-vs.-time curves are shown in panels c and d of Fig. 11 for the Gaussian and GH treatments, respectively. Ideally, these curves should be horizontal lines lying atop one another, but this is only approximately true in practice. Overall, as expected, the deduced FOM value is least dependent on the choice of transducer when the more accurate GH beam model is used.

The effect of the beam model choice on the deduced FOM value is more explicitly demonstrated in

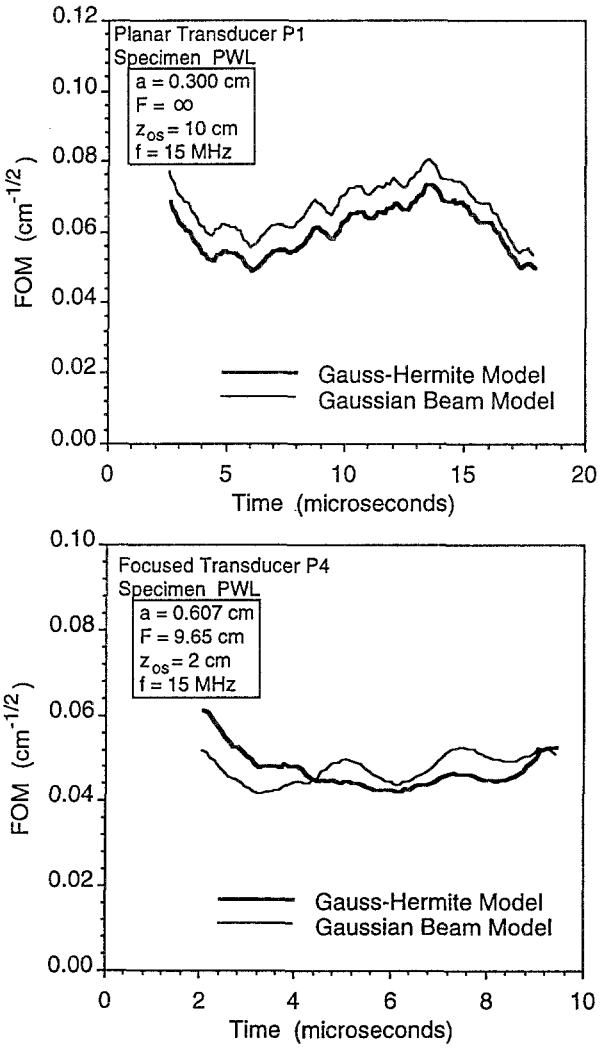

Fig. 12. Effects of beam-model choice on deduced FOM values. Inspection particulars are those for transducers P1 and P4 in Fig. 11.

Fig. 12 for transducers P1 (planar) and P4 (focused). The choice of beam model determines the value of the beam integral $G(z_1)$ which, in turn, impacts the deduced FOM. The relevant beam integrals for transducers P1 and P4 in this setting were previously displayed in Fig. 7. For each transducer, one can observe a clear correspondence between the differences in beam integral values for the Gaussian and GH calculations (Fig. 7) and the differences in extracted FOM values (Fig. 12).

The toneburst noise model can be used to predict the rms noise level in each experiment if a value for the FOM is assumed. Such predictions for transducers P1-P5 are presented in Fig. 11e, using the GH beam model and assuming FOM=0.048 cm$^{-1/2}$ at 15 MHz. This FOM value is an average of the extracted values shown in Fig. 11d. The overall agreement between measured and predicted noise level curves is seen to be quite good. This indicates that the model can properly account for the effects of beam focusing and diffraction on the backscattered noise level. Recall that the present model calculations assume that the effective attenuation of the metal is negligible. An alternative analysis of the 5-transducer data, assuming α_1=0.07cm^{-1} at 15 MHz, may be found in Ref. 10. There, the influence of attenuation causes the mean extracted FOM value to be somewhat higher (0.060 cm$^{-1/2}$), but the predicted $N(t)$ curves differ only modestly from those shown in Fig. 11e of the present work.

Experiments were also carried out to test the ability of the model to predict the changes in noise levels that result from a lengthening of the toneburst duration. The results of this study are summarized in Fig. 13. Four experimental trials were conducted using focused transducer P4 positioned above side 4 of specimen PWL. All measurement system parameters were the same for the four trials, except for the duration of the incident 15-MHz toneburst pulse. The front-surface reference echo for each trial is shown in panel a of Fig. 13; these echoes are seen to have similar peak amplitudes, and to have durations of approximately 1, 2, 3, and 4 microseconds, respectively. For each trial 500 backscattered noise signals were acquired and analyzed, and the resulting normalized rms noise levels are displayed in panel b. Equations (15)–(18) predict that the noise level at any fixed time is approximately proportional to the square root of the toneburst duration. Notice that the observed noise level for the 4 μsec pulse is about twice that of the 1 μsec pulse, as expected. FOM values extracted from the measured noise data (assuming the Gaussian beam model) and subsequent noise level predictions are shown in panels c and d of Fig. 13. The agreement seen between panels b and d indicates that the noise model can successfully predict the *relative* effects of both beam focusing the toneburst duration on the backscattered noise level. Moreoever, the predictions are reasonably accurate even when the simple Gaussian beam model is used. Note that the absolute noise level is determined by the FOM which plays the role of a scaling constant, and we are determining this constant by using our model to analyze backscattered noise data. Thus we are, in reality, only testing the ability of the model to predict the change in noise level that occurs when some inspection parameter is altered, e.g., the observation time or toneburst duration.

In noise measurement experiments with a given transducer we can expect to see two types of changes when the toneburst frequency is altered: (1) the overall magnitude of the noise will change, due to the frequency

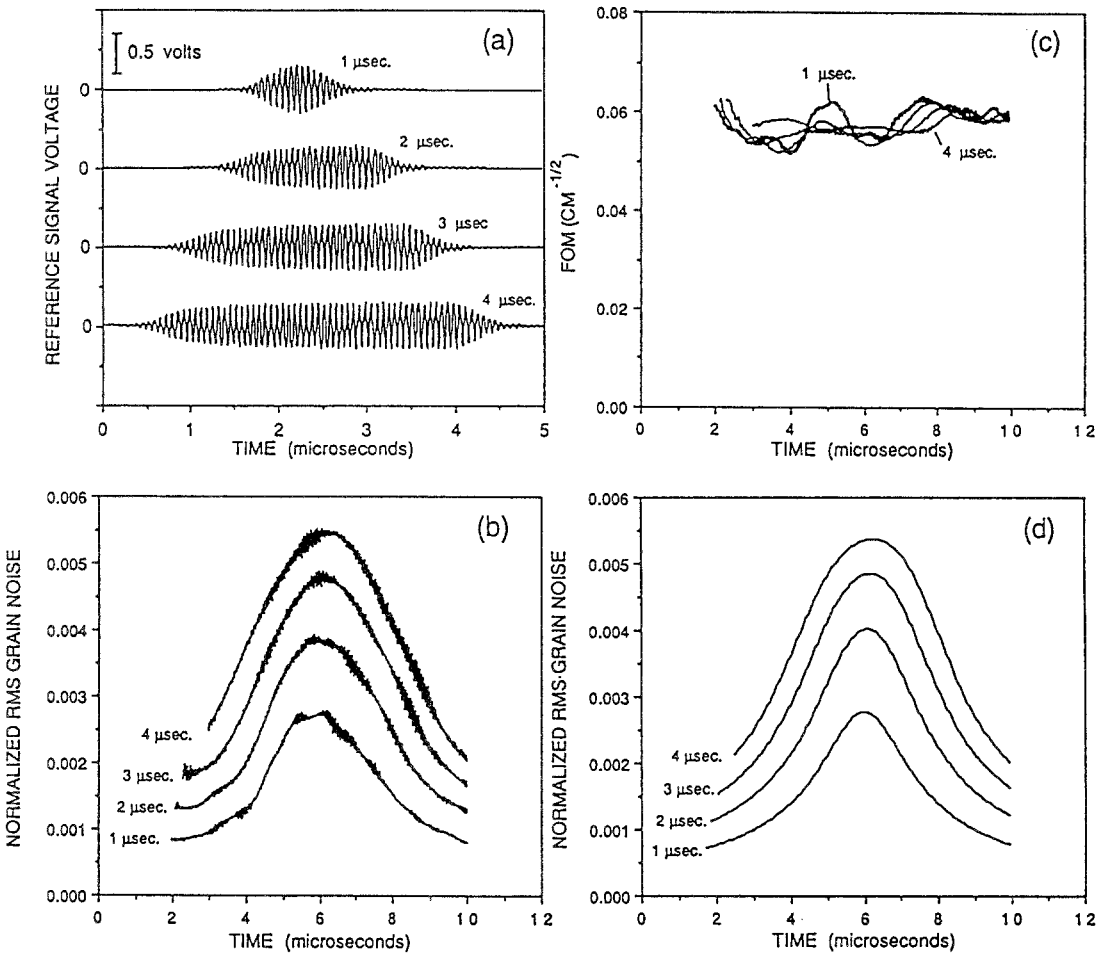

Fig. 13. Effect of toneburst duration on backscattered noise: specimen PWL side 4; transducer P4; z_{0R}=9.65 cm; z_{0S}=3.0 cm; f=15MHz. (a) Front surface reference signals used in four successive experimental trials. (b) Measured normalized rms noise level for each trial. (c) FOM at 15 MHz extracted from noise data using Eq. (15) (α_1=0; Gaussian beam model; 5-point smoothing). (d) Predicted normalized rms noise levels for the four trials using Eq. (15) and FOM=0.056 cm$^{-1/2}$ (α_1=0; Gaussian beam model). For panels (b), (c), and (d), t=0 is the time at which the center of the front-surface echo is seen when the waterpath is z_{0S}; a different time origin is used for panel (a). The minor wiggles on the curves in panel (d) are manifestations of the plotting program; smooth curves are predicted by the theory.

dependence of the average single-grain backscattering amplitude, and (2) the time dependence of $N_{rms}(t)$ will be altered by the modification of the incident beam profile (e.g., the narrowing of the focal zone with increasing frequency). To test the ability of the noise model to predict changes in the shape of $N_{rms}(t)$, side 2 of specimen PWL was insonified using tonebursts of similar duration (~1 μsec) but differing frequency (10, 15, and 20 MHz). The measured rms noise level was observed to increase rapidly with frequency, and shape changes were also seen. The measured and predicted time-dependences of the $N_{rms}(t)$ curves are compared in Fig. 14, where each curve has been rescaled to a peak amplitude of unity to better compare the shapes. As the transducer oscillation frequency is increased, the beam in the metal becomes more tightly focused, and the point of maximum pressure amplitude moves outward, approaching the geometric focal point. The time of occurrence of the broad focal peak in the rms noise, its shift to the right, and its sharpening with increasing frequency are well predicted by the toneburst noise model. In addition to changes association with the sharpening of the beam focus, the shape of $N_{rms}(t)$ is influenced by the value of the metal attenuation coefficient which appears in the $\exp(-4\alpha_1 z_1)$ term in Eq. (15). The increase of attenuation with frequency acts to suppress the late arriving noise, and hence to shift the noise peak to earlier times. This effect was not appreciable in specimen PWL due to its small effective attenuation and limited thickness. Detailed analysis of Fig. 14 indicates that the use of the GH beam

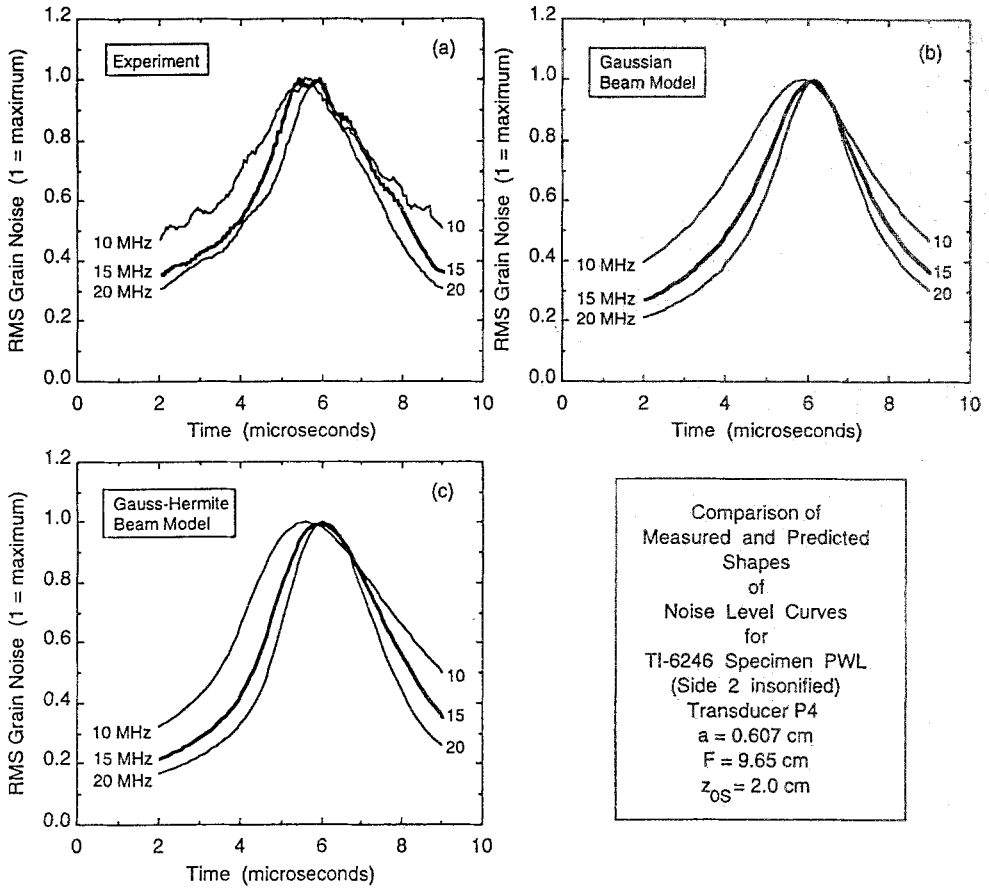

Fig. 14. Measured (a) and predicted (b and c) rms noise levels for 10, 15, and 20 MHz toneburst inspections of specimen PWL. Noise predictions use the Gaussian (b) or Gauss-Hermite (c) beam model with $\alpha_1=0$ and assume the fitted transducer parameters of P4.

model results in better agreement with experiment near the broad peaks of the three $N_{\text{rms}}(t)$ curves, and that the Gaussian beam results are more accurate in the tails. In our various tests of the noise model, predictions made using the GH beam model were generally found to be more accurate than their Gaussian counterparts near the focal zone of each focused transducer. However, little overall accuracy was lost by employing the simpler beam model.

7. THE DETERMINATION OF EFFECTIVE ATTENUATION

The practical use of the toneburst noise model, to extract the FOM of a specimen or to predict noise levels given the FOM, requires that the ultrasonic attenuation of the metal be known at the inspection frequency. We now briefly discuss three methods for determining α_1, and apply each to Ti-6246 specimen PWL (for sound propagation perpendicular to sides 1 and 4). The methods are summarized in Fig. 15, and full details can be found in Ref. 15.

A common method for measuring attenuation is based on the deconvolution of surface echoes which have different round-trip travel distances through the specimen. The use of the first and second back surface (BS) echoes is illustrated in Fig. 15a. The echoes are generally acquired using a planar transducer which emits a broadband sonic pulse. Applying the paraxial measurement model in the spirit of Eq. (7), the magnitude of the spectral component for the mth back surface echo may be written as

$$|\Gamma_{\text{BS}m}(\omega)| = |\beta(\omega)T_{01}R_{11}^{2m-1}T_{10}D_{\text{BS}m}(\omega)|\, e^{-2\alpha_0 z_0 - 2m\alpha_1 h_1} \tag{23}$$

where z_0 is a one-way waterpath, h_1 is the specimen thickness, $D_{\text{BS}m}$ is a diffraction correction factor, and T_{01}, T_{10}, and R_{11} are plane-wave transmission and reflection coefficients. $D_{\text{BS}m}$ can be evaluated by setting $S=4\pi$

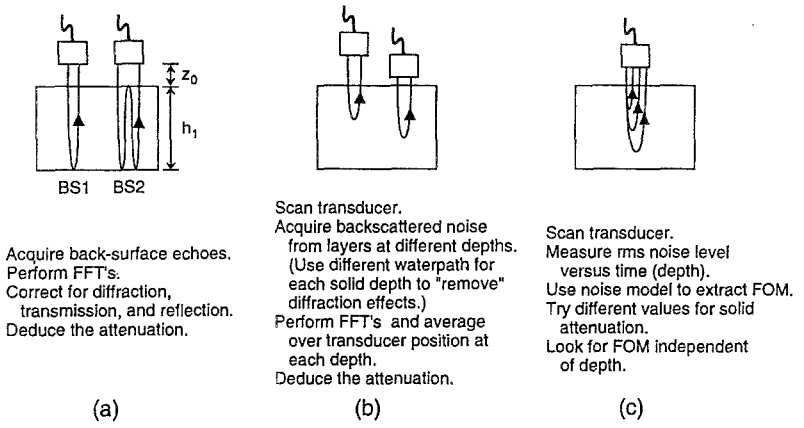

Fig. 15. Three immersion methods for determining the ultrasonic attenuation α_1) of a metal specimen. Method (a) makes use of multiple back-surface echoes. Methods (b) and (c) make use of backscattered noise echoes.

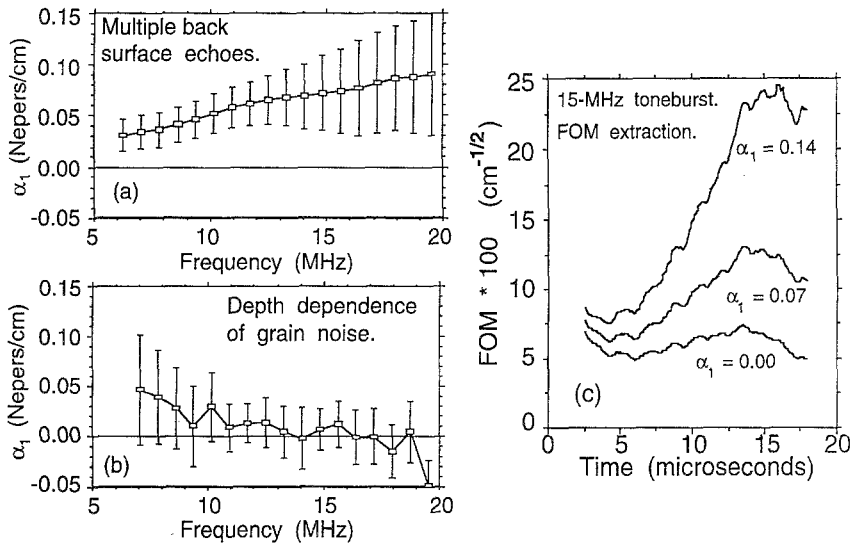

Fig. 16. Estimating the effective attenuation of Ti-6246 specimen PWL by (a) analyzing back surface echoes, (b) analyzing the depth dependence of noise, and (c) examining the time-dependence of deduced FOM.

$(z_0v_0+mh_1v_1)/\omega a^2$ in Eq. (20), and R_{11} may be found from $R_{11}=-R_{00}$ and Eq. (19). If Eq. (23) is applied to each of two distinct BS echoes, the common factor of $\beta T_{01}T_{10}\exp(-2\alpha_0 z_0)$ may be eliminated, and $\alpha_1(\omega)$ subsequently deduced from the measured ratio of spectral components.

In our application of this technique to specimen PWL, the first two BS echoes were recorded at 135 locations above side 4 using a 15-MHz, broadband, planar transducer (a=0.60 cm, z_0=8.0 cm). At each location, Eq. (23) was used to determine α_1 at each frequency for which both echoes had sufficient spectral strength, approximately 6 MHz≤f≤20 MHz. The 135 values of α_1 obtained at each frequency were then analyzed to determine their mean and standard deviation. These are displayed in Fig. 16a. Large variations in the strength and appearance of the BS echoes were observed as the transducer was scanned above the specimen. These variations are responsible for the large standard deviations evident in the figure, and are believed to result from phase-front distortion by velocity variations between neighboring macrostructural elements (prior beta grains). The diffraction corrections used in Eq. (23) assume that the wavefronts arriving at the receiver have been distorted (i.e., curved) by the usual beam-spreading phenomenon which occurs during propagation through homogeneous,

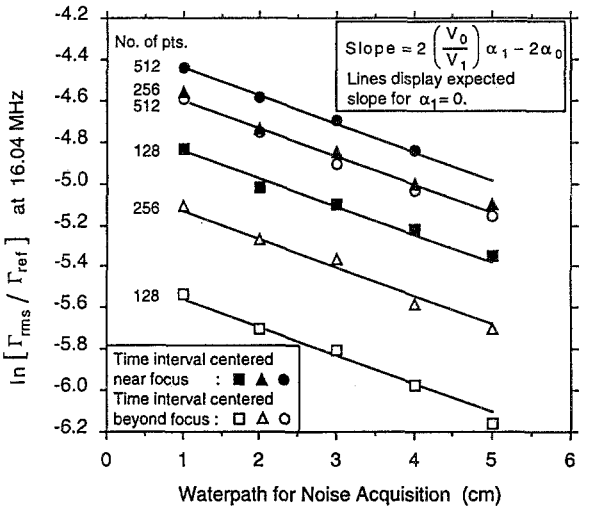

Fig. 17. Logarithmic plot of the rms spectral component of the backscattered noise at 16.04 MHz vs. the waterpath. Six sets of results are shown corresponding to the six choices of the analysis time window for the initial waterpath. The solid lines are not best fits through the data, but merely display the expected slope if $\alpha_1=0$ (Transducer P4; Specimen PWL; side 4).

isotropic media. Additional wavefront distortion, caused by different portions of the beam traveling at different average velocities through the solid, would lead to deduced α_1 values which are too high.

In the second method, attenuation values were deduced by examining backscattered broadband noise echoes from layers at different depths in the specimen. The procedure used is similar to that of Nagy, Rypien, and Adler,[4] except we vary the waterpath to correct for diffraction effects. Briefly, using a fixed waterpath of z_0 and a broadband incident pulse, we scan the transducer laterally to acquire noise echoes at many locations. Using a time window of fixed duration, with center time t_c after the FS echo, the FFT of each noise echo is performed and the rms average spectral component, denoted $\Gamma_{rms}(\omega)$, is calculated at selected frequencies. If the backscattered noise arises primarily from single scattering, the noise observed in the time window originates from a layer of grains whose center is located at a depth of $z_{1c}=t_c v_1/2$. We then simultaneously change the waterpath and the center of the FFT window in such a way that $z_0+z_{1c}(v_1/v_0)$ remains constant. In the absence of attenuation, the radiation pattern in the solid layer is then approximately the same for all layers studied. Hence, changes in the rms noise spectrum observed when the waterpath (and t_c) are varied are ascribed to the effects of attenuation. In particular, at a given frequency, Γ_{rms} is assumed to be proportional to $\exp[-2z_0\alpha_0-2z_{1c}\alpha_1]$ and hence to $\exp[-2z_0(\alpha_0-v_0\alpha_1/v_1)]$. Thus, α_1 can be deduced from the slope of a plot of $\ln(\Gamma_{rms})$ vs. waterpath if the attenuation of water is known. Note that the method does not require knowledge of the radius and focal length of the transducer.

In our application of the method to specimen PWL, broadband focused transducer P4 was used and backscattered noise echoes were acquired at 500 locations above side 4 at each of 5 waterpaths. The attenuation extraction procedure was then carried out for each of six choices of the initial FFT time window. At the first waterpath (z_0=1.0 cm) the time window was either centered near the focus (tc=6.8 μsec) or beyond the focus (tc=9.0 μsec) and had a duration of either 1.27, 2.55, or 5.11 μsec (leading to 128, 256, or 512 discrete points at our 100 MHz sampling rate). The initial choice of z_0 and tc determines the center of the corresponding time windows for the other waterpaths. The measured values of Γ_{rms} (normalized by the spectral component of our usual FS reference signal) at 16.04 MHz are shown in Fig. 17 for each waterpath and each choice of the initial FFT window. As expected, the data points appear to be linearly related when plotted as $\ln[\Gamma_{rms}]-vs-z_0$, and the slope is nearly independent of the choice of the initial time interval. For each choice of time interval in Fig. 17, a "best fit" straight line can be drawn through the data, and α_1 can be determined from the slope of this line and the known attenuation of water at the temperature of the experiment. We used Pinkerton's values for the attenuation of water[30] after verifying that they agreed with measurements made at one temperature on the filtered tap water used in our experiments. Six values of α_1 result from the analysis at 16.04 MHz and the mean and standard deviation of these values are displayed in Fig. 16b, together with those obtained by similar analyses at other frequencies. The figure indicates that the effective attenuation of specimen PWL, as deduced from the depth dependence of backscattered noise, is consistent with $\alpha_1=0$ on 10 MHz$\leq f\leq$20 MHz.

Note that the linearity of the $\ln[\Gamma_{rms}]-vs-z_0$ plot in a given specimen is an indicator of the applicability of our single-scattering noise model there. In general, a multiple scattering event involving a given grain has a longer round-trip traver path in the solid than the single-scattering event for the same grain. Thus, the early time noise signals can be expected to primarily arise from single-scattering, with the effects of multiple scattering being more pronounced at later times.[21] If multiple scattering processes are important, $\ln[\Gamma_{rms}]-vs-z_0$ may be approximately linear for near-front-surface scattering

(larger z_0), but excess noise may be observed at later times (smaller z_0), resulting in a curvature of the $\ln[\Gamma_{rms}-vs-z_0$ data. We have observed such curvature for a copper specimen.[15] However, no such curvature was seen for Ti-6246 specimen PWL, indicating that the single-scattering assumption is valid for that specimen and our inspection frequency.

The deduction of α_1 from backscattered noise by the method just described requires no detailed model for backscattered noise, nor any knowledge of the incident radiation pattern in the metal. However, since we possess a noise model (Eq. 15) and well-characterized transducers, an alternative method of deducing α_1 from backscattered noise may be pursued. One can perform a toneburst insonification of the specimen, measure the normalized rms noise level as a function of time, and then use the noise model to repeatedly extract the FOM from the measured noise level, assuming different values of α_1 for each extraction. One then selects the value of α_1 for which the extracted FOM is least dependent on time. This method is demonstrated in Fig. 16c. Backscattered noise echoes were earlier acquired through side 4 of specimen PWL using planar transducer P1 emitting a 1-μsec 15-MHz toneburst (see Fig. 11b). Equation (15) was used to determine the FOM as a function of time, assuming α_1 values of 0, 0.07, and 0.14 nepers/cm at 15 MHz. In Fig. (16c), the FOM is seen to be at least dependent on time for the $\alpha_1=0$ extraction, and thus in agreement with the results of Fig. 16b.

The effective attenuation, α_1, which appears in the noise model, may be viewed as a material-dependent parameter which plays a role in the time (or depth) dependence of the backscattered noise. Our studies indicate that the value of α_1 which leads to the best performance of the model may be different than the value determined by traditional means. Here the traditional measurement method leads to a deduced attenuation coefficient which rises linearly with frequency. Such linear behavior is not seen in the Rayleigh regime where the mean size of the effective scatterers is small compared to the wavelength. Rather, it is likely that we are near the top of the stochastic regime where the scattering is mostly forward oriented. The situation is analogous to the forward scattering induced by surface roughness, studied by Nagy and Adler.[5] The roughness causes phase perturbations in the metal which can greatly reduce coherent surface echoes without leading to a corresponding reduction in the incoherent backscattered noise. Thus the attenuation coefficient deduced from surface echoes can greatly overstate the attenuation coefficient appropriate for backscattered noise.

8. FOM EXTRACTION IN SIMPLE MICROSTRUCTURES

For most materials it is not currently feasible to deduce the FOM by any means other than analyzing backscattered noise. Photographic examinations of the microstructure may provide information about the distribution of grain sizes, but other quantities which determine the average single-grain scattering amplitude may not be known or readily deduced. These quantities include the single-crystal elastic constants for each phase in the presence of alloying elements, the orientation distribution functions for the principal axes of the grains, and the degree to which grains of similar properties and orientations "clump together" to form larger effective scatterers. Consequently, it is not generally possible to conduct an absolute test of the noise model, in which the FOM deduced from the rms noise level is compared with the value deduced independently from knowledge of the microstructure. However, such comparisons are feasible if the microstructure is simple, and we now report preliminary results for five single-phase metal specimens having approximately equi-axed, randomly-oriented grains. The five specimens are denoted SS (fine-grained 304 cast stainless steel), CU (commercially pure, cast copper) and TIA, TIB, and TIC (pure alpha-phase titanium from hipped powder). In an attempt to produce three titanium specimens with significantly different mean grain sizes, the metal powder was sifted prior to hipping to obtain three mixtures with different mean particle sizes. However, the powder particles themselves were later found to generally be composed of several grains each, and the restrictions on particle diameters consequently had little effect on grain diameters in the finished specimens. A fuller account of the specimens, and the measurements performed on them is contained in Ref. 15.

To estimate the FOM from microstructure, we make use of the work of J. H. Rose, [21,22] who had conducted a formally rigorous analysis of the backscattered noise problem for early times, before multiple-scattering effects become important. His work assumes that the wavelength is much larger than the mean grain sizes, and that the scattering is relatively weak so that the Born approximation can be employed. The scattering from a single grain is calculated by embedding that grain in an "effective medium" formed by the neighboring grains. Rose demonstrates that the propoerties of the effective medium are obtained from Voigt averages of the single-grain elastic constants, and he relates the FOM of a specimen to details of its microstructure. For L-wave

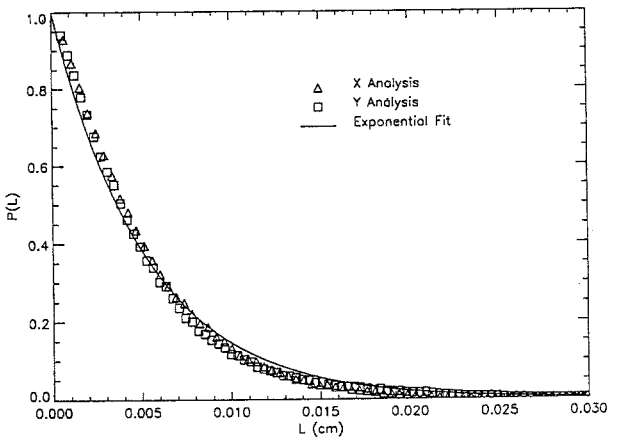

Fig. 18. $P(L)$, the probability that an arbitrary line segment of length L is enclosed within a single grain. Plotted points result from two analyses of a photograph of the microstructure of specimen SS, one using line segments aligned with the X-axis of the photo, and the other using segments aligned with Y. The fitted exponential function is $P(L)=\exp(-L/b)$ with $b=52$ μm.

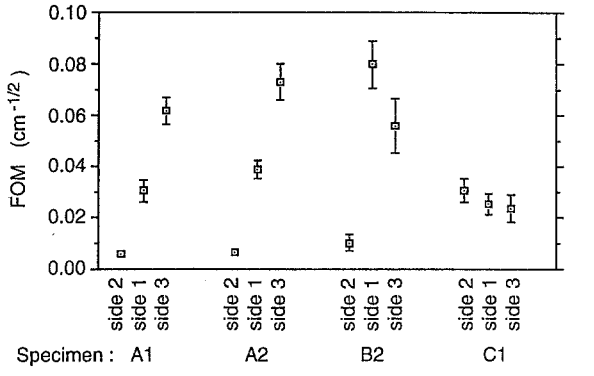

Fig. 19. Figure-of-Merit for grain noise severity. Values at 15 MHz for four Ti-6246 specimens.

backscatter from an equi-axed distribution of randomly-oriented grains, Rose's results may be written as[15]

$$\text{FOM} = \left[\frac{\pi^2 f^3 <(\delta C_{33})^2>}{\rho^2 v^7}\int_0^\infty L\sin\left(\frac{4\pi f L}{v}\right)P(L)dL\right]^{1/2} \tag{24}$$

where ρ is the density, f is the frequency, v is the Voigt-averaged longitudinal velocity, and $<(\delta C_{33})^2>$ is the square of the difference between the 33 elastic constant of the effective medium and that of a single grain, averaged over all grain orientations. $P(L)$ is the probability that a line segment of length L, arbitrarily placed in the specimen, is entirely enclosed by a single grain. If the crystallites possess cubic symmetry (e.g., stainless steel or copper), then

$$v = [(3C_{11}+2C_{12}+4C_{44})/(5\rho)]^{1/2} \tag{25}$$

and

$$<(\delta C_{33})^2> = 16[C_{11}^2-2C_{11}C_{12}+C_{12}^2-4C_{11}C_{44} +4C_{12}C_{44}+4C_{44}^2]/525 \tag{26}$$

where the C_{ij} are single-crystal elastic constants in a principal-axis coordinate system aligned with the edges of the cubic cell. For hexagonal symmetry (e.g., alpha-titanium), then

$$v = [(8C_{11}+3C_{33}+4C_{13}+8C_{44})/(15\rho)]^{1/2} \tag{27}$$

and

$$\begin{aligned}<(\delta C_{33})^2> = [&192C_{11}^2-128C_{11}C_{13} \\ &+48C_{13}^2-256C_{11}C_{33} \\ &+32C_{13}C_{33} \\ &+112C_{33}^2-256C_{11}C_{44} \\ &+192C_{13}C_{44} \\ &+64C_{33}C_{44} \\ &+192C_{44}^2]/1575\end{aligned} \tag{28}$$

assuming that the third (z) principal axis is the six-fold symmetry axis. Thus, for single-phase, equi-axed, randomly-oriented materials, the determination of the FOM from microstructure requires knowledge of the density, the single crystal elastic constants, and the probability for line segment enclosure, $P(L)$.

For the three materials in question, estimates of the relevant elastic properties were obtained from the literature.[15,31-33] For each specimen, a discrete approximation of $P(L)$ was obtained by analyzing a digitized image of the microstructure. In the image, apparent twin boundaries were first suppressed. Then, using computer software, many line segments of a fixed length L were randomly placed on the image, and each segment was examined to determine whether or not it crossed a grain boundary. This allowed us to determine the probability that a segment of that length would lie in a single grain. This process was repeated for approximately 75 choices of the line segments length to estimate $P(L)$ over the relevant range of L. An example of the resulting set of $P(L)$ values is shown in Fig. 18.

When determining the FOM from Eq. (24), two methods were used to evaluate the integral over L. In the first, the integration was performed numerically using the discrete $P(L)$ function. In the second, the integration was performed analytically by assuming $P(L)=\exp(-L/b)$, with the parameter b determined by an exponential fit to the discrete function. The metallographically-determined FOMs at selected frequencies are listed in Table I for the five equi-axed specimens. Other

Table I. Comparison of FOM Values Deduced from Metallographic Analysis and from Backscattered Ultrasonic Noise

Specimen designation	Material	Number of grains in photograph	Average grain radius (μm)[a]	Frequency for FOM determination (MHz)	Metallographic FOM ($cm^{-1/2}$)[b,c] (2)	(3)	Ultrasonic FOM ($cm^{-1/2}$)
SS	Stainless steel	154	52.0	5	0.0326	0.0357	0.029–0.035
CU	Copper	123	112.3	5	0.0584	0.0548	0.025–0.053
TIA	α-titanium	192	20.2	15	0.0203	0.0215	0.033–0.039
TIB	α-titanium	226	15.8	15	0.0150	0.0168	
TIC	α-titanium	195	16.0	15	0.0163	0.0180	

[a] Radius quoted is the value of b in the fitted function $P(L)=e^{-L/b}$.
[b] FOM in column (2) results from the numerical integration of the measured $P(L)$.
[c] FOM in column (3) results from integration of the fitted function, $P(L)=e^{-L/b}$.

Table II. Further Heat Treatment of Ti-6246 Specimens[a]

Specimen	Anneal temperature	Anneal time	Cooling method
A1	1670°F	1 hr	Air cool
A2	1745°F	1 hr	Air cool
B2	1745°F	8 hr	Water quench
C1	1795°F	1 hr	Air cool

[a] Beta transus = 1775°F.

pertinent data, including the approximate number of grains in each image, are also given. Grain boundaries were less distinct in the titanium photos, than in the copper and stainless steel ones. The differences in tabulated FOM values for the three titanium specimens probably are not primarily due to differences in the grain size distributions of the specimens. Rather, they likely arise from difficulties in assigning grain boundaries, and from the inherent uncertainty in deducing $P(L)$ from a single photograph containing a limited number of grains.

In the far righthand column of Table I, we list the FOM values extracted from measured backscattered noise using the method described in Section 5. The range of values indicated for each specimen arises from the dependence of the deduced FOM value on the time (or depth) at which the extraction was performed, on the choice of effective attenuation, and (for copper) on the choice of transducer. Focused transducers were used for the majority of the noise measurements, and in all cases at least two attenuation measurement procedures (deconvolution of surface echoes, and time dependence of extracted FOM) were used to estimate reasonable values for α_1. Notice that a different inspection frequency (15 MHz) was used for the titanium specimens than for copper and steel (5 MHz). For titanium, the backscattered noise level seen in 5-MHz inspections (and hence the FOM value at 5 MHz) was too small to be accurately measured using our apparatus.

Little difference was seen in the backscattered noise levels of the three titanium specimens, or in their extracted FOM values. There was evidence that secondary scattering effects were not negligible in the copper specimen (high attenuation, curvature in $\ln\Gamma_{rms}-vs-z_0$ plots, differences in FOM values deduced using planar and focused transducers), and more credence was consequently placed on FOM values extracted at early times. The metallographically and ultrasonically determined FOM values agree to within a factor of two for each specimen listed in Table I, and this level of agreement is gratifying given that: (1) no adjustable parameters are involved in either determination, (2) grain boundary assignments are somewhat subjective, and (3) measured noise levels in these specimens are 60 dB or more below the front surface reference signal. Thus, our preliminary results indicate that the ultrasonic FOM for noise severity can be predicted with reasonable accuracy (±6 dB) from first principles for simple microstructures.

9. EXTRACTED FOM'S FOR TI-6246 SPECIMENS

Toneburst measurements were carried out to assess noise severity in titanium materials of the type used in aircraft engine components. Four Ti-6246 specimens (designated A1, A2, B2, and C1) were studied in detail.[17] The starting point for each specimen was VAR melted material processed to an equi-axed alpha-beta microstructure at 6-inch diameter billet. Further heat treatment utilized to modify the microstructure is summarized in Table II. Note that the beta transus for this alloy

is 1775°F, so that the first three samples were annealed below the beta transus while the fourth was annealed above it. Like PWL discussed earlier, these specimens displayed structure on at least two length scales: microstructural elements (grains) had average dimensions on the other of 10 μm; macrostructural elements (prior beta grains) had average dimensions of several millimeters or more. Velocity, attenuation, and backscattered noise measurements were made through three mutually orthogonal sides of each specimen. The noise measurements employed focused transducer P5 (see Fig. 11a) and used 15-MHz tonebursts of 1 μsec duration. The dependence of longitudinal wave velocity on propagation direction was minimal (≤0.5%) in each specimen, but the backscattered noise level was strongly dependent on direction in three of the specimens. The deduced FOM values at 15 MHz and their estimated uncertainties are displayed in Fig. 18. The noise anisotropy documented in that figure is believed to arise from localized texture within macrostructural elements,[15,29] and is a topic of ongoing research.

10. SUMMARY AND CONCLUSIONS

We have presented a model for backscattered ultrasonic noise in weakly-scattering materials, which assumes that the noise is an incoherent sum of direct echoes from individual grains. The model relates the absolute rms noise level observed in a toneburst immersion inspection to details of the measurement system, and to a factor (FOM) which depends on the microstructure of the specimen. The model can be used to deduce the FOM of a specimen from measured noise data, or, if the FOM is known, to predict the absolute noise level which would be seen under various inspection scenarios. Validation studies, conducted using both synthetic noise signals and noise measured in commercial titanium alloys, demonstrate that the model can successfully explain the dependence of the noise level on depth for both planar and focused transducers, and on toneburst duration and frequency. In separate studies on specimens with simple microstructures, FOM values deduced from backscattered noise were found to be in reasonable agreement with values estimated independently from knowledge of the microstructure.

Model terms pertaining to the incident ultrasonic displacement field in the solid have been evaluated using either a Gaussian or Gauss-Hermite beam model. For focused transducers in the vicinity of the focal zone (where noise levels are highest), noise level predictions made using the Gaussian and GH models are found to differ by ≤10%. Since the typical "accuracy" of the noise model, as gauged by the difference between theory and experiment in practice, is also of this order, it is not unreasonable to use the simpler Gaussian model for most beam calculations. For the Gaussian case, all formulas required for implementation of the noise model have been explicitly stated in Section 3.

A version of the model appropriate for broadband ultrasonic pulses can be developed by using Eqs. (7) and (8) and the incoherent superposition assumption to obtain an expression for the rms spectral components of the noise on a finite time interval. Parseval's theorem can then be used to relate these components to the rms noise level in the interval. Our own efforts along these lines may be found in Refs. 15 and 34, and a similar approach has been pursued by Russell and Neal.[11–14] When broadband pulses are used, data analysis is more complicated (FFT operations are performed on all noise waveforms), but the FOM of the specimen is deduced over a range of frequencies. The extension of the model to cover inspection through curved boundaries is essentially accomplished by modifying the focusing/diffraction factor, C, in Eq. (16). Again an analytic expression for $G(z)$ results when the Gaussian beam model is used.[35] The underlying model can be extended to oblique incidence by considering separate longitudinal and shear wave beams in the metal, each of which contributes additively to the mean squared noise level or mean power spectrum. This concept has been tested by Russell and Neal using titanium specimen TIA.[14]

By using Eq. (15) to estimate the rms noise level, and Eqs. (7) and (8) to estimate the amplitude of the backscattered echo from a hypothesized defect, signal-to-noise (S/N) ratios for ultrasonic inspections can be estimated. We have used this approach to predict S/N ratios for "hard-alpha" defects of various sizes in titanium alloys.[10,15] If the Gaussian beam model is used in both the defect signal and noise level calculations, and if certain additional approximations are made, simple formulas can be developed which allow rapid "back-of-the-envelope" estimates of S/N ratios. The application of such formulas to the spection of cylindrical billets is discussed in Ref. 35.

ACKNOWLEDGMENTS

The majority of this work was supported by the Center for Advanced Nondestructive Evaluation, operated by the Ames Laboratory, USDOE, for the Air Force Wright Laboratory/Materials Directorate under Contract No. W-7405-ENG-82 with Iowa State University. Cer-

tain measurements and analyses pertaining to the deduction of the Figure-of-Merit from microstructure (Section 8), and the preparation of the manuscript itself were supported by the FAA-Center for Aviation Systems Reliability, operated by the Ames Laboratory, USDOE, for the Federal Aviation Administration under Contract No. W-7405-ENG-82 with Iowa State University.

The authors wish to thank Seth Meyer and Scot Goettsch for assisting with experimental measurements, Kim Han for digitizing microstructure photographs and making initial demonstrations of the procedure for determining P(L), Lisa Brasche for supervising the production of powder metallurgy specimens, and James H. Rose for illuminating discussions on the relationship between microstructure and the Figure-of-Merit for noise severity.

REFERENCES

1. A. B. Bhatia, *Ultrasonic Absorption* (Chap. 11) (Clarendon Press, Oxford, 1967).
2. K. Goebbels, Structure analysis by scattered ultrasonic radiation in *Research Techniques in Nondestructive Testing*, R. S. Sharpe, ed. (Academic Press, New York, 1980), pp. 87–157.
3. B. R. Tittmann and L. Ahlberg, Attenuation and grain noise parameters in Ni-base alloys in *Review of Progress in Quantitative NDE*, Vol. 2A, D. O. Thompson and D. E. Chimenti, eds. (Plenum Press, New York, 1983), pp. 129–145.
4. P. B. Nagy, D. V. Rypien, and L. Adler, Ultrasonic attenuation measurement by backscattering analysis in *Review of Progress in Quantitative NDE*, Vol. 6B, D. O. Thompson and D. E. Chimenti, eds. (Plenum Press, New York, 1987), pp. 1411–1417.
5. P. B. Nagy and L. Adler, Scattering induced attenuation of ultrasonic backscattering, in *Review of Progress in Quantitative NDE*, Vol. 7B, D. O. Thompson and D. E. Chimenti, eds. (Plenum Press, New York, 1988), pp. 1263–1271.
6. E. L. Madsen, M. F. Insana, and J. A. Zagzebski, Method of data reduction for accurate determination of acoustic backscatter coefficients, *J. Acoust. Soc. Am.* **76:**913–923 (1984).
7. M. F. Insana, E. L. Madsen, T. J. Hall, and J. A. Zagzebski, Tests of accuracy of a data reduction method for determination of acoustic backscatter coefficients, *J. Acoust. Soc. Am.* **79:**1230–1236 (1986).
8. T. J. Hall, E. L. Madsen, J.A. Zagzebski, and E. J. Boote, Accurate depth-independent determination of acoustic backscatter coefficients with focused transducers, *J. Acoust. Soc. Am.* **85:**2410–2416 (1989).
9. F. J. Margetan, T. A. Gray, and R. B. Thompson, A technique for quantitatively measuring microstructurally induced ultrasonic noise, in *Review of Progress in Quantitative NDE*, Vol. 10B, D. O. Thompson and D. E. Chimenti, eds. (Plenum Press, New York, 1991), pp. 1721–1728.
10. F. J. Margetan and R. B. Thompson, Microstructural noise in titanium alloys and its influence on the detectability of hard-alpha inclusions, *Review of Progress in Quantitative NDE*, Vol. 11B, D. O. Thompson and D. E. Chimenti, eds. (Plenum Press, New York, 1992), pp. 1717–1724.
11. M. D. Russell, S. P. Neal, and E. J. Boote, Experimental estimation of the longitudinal-wave backscatter coefficients for ultrasonic interrogation of weak scattering materials, *J. Acoust. Soc. Am.* **93:**1267–1276 (1993).
12. M. D. Russell and S. P. Neal, Experimental estimation of the transverse-wave backscatter coefficients for ultrasonic interrogation of weak scattering materials, *J. Acoust. Soc. Am.* (to be published).
13. M. D. Russell and S. P. Neal, Grain noise power spectrum estimation for weak scattering polycrystalline materials using experimentally estimated backscatter coefficients: Normal incidence, *Ultrasonics* (to be published).
14. M. D. Russell and S. P. Neal, Grain noise power spectrum estimation for weak scattering polycrystalline materials using experimentally estimated backscatter coefficients: Oblique incidence, *Ultrasonics* (submitted).
15. F. J. Margetan, R. B. Thompson, I. Yalda-Mooshabad, and Y. K. Han, Detectability of Small Flaws in Advanced Engine Alloys, U.S. Air Force Technical Report, Center for NDE, Iowa State University, Ames, Iowa (1993).
16. F. Amin, T. A. Gray, and F. J. Margetan, A new method to estimate the effective geometric focal length and radius of ultrasonic focused probes, in *Review of Progress in Quantitative NDE*, Vol. 10A, D. O. Thompson and D. E. Chimenti, eds. (Plenum Press, New York, 1991), pp. 861–865.
17. Specimen PWL was supplied by Pratt & Whitney Aircraft, West Palm Beach, Florida; Specimens A1, A2, B2, and C1 were supplied by General Electric AEBG, Cincinnati, Ohio.
18. I. Yalda-Mooshabad, F. J. Margetan, and R. B. Thompson, Monte-Carlo simulation of ultrasonic grain noise, in *Review of Progress in Quantitative NDE*, Vol. 12B, D. O. Thompson and D. E. Chimenti, eds. (Plenum Press, New York, 1993), pp. 1727–1734.
19. R. B. Thompson and T. A. Gray, A model relating ultrasonic scattering measurements through liquid–solid interfaces to unbounded medium scattering amplitudes, *J. Acoust. Soc. Am.* **74:** 1279 (1983).
20. B. A. Auld, General electromechanical reciprocity relations applied to the calculation of elastic wave scattering coefficients, *Wave Motion* **1:**3 (1979).
21. J. H. Rose, Ultrasonic backscatter from microstructure, in *Review of Progress in Quantitative NDE*, Vol. 11B, D. O. Thompson and D. E. Chimenti, eds. (Plenum Press, New York, 1992), pp. 1677–1684.
22. J. H. Rose, Theory of ultrasonic backscatter from multiphase polycrystalline solids, in *Review of Progress in Quantitative NDE*, Vol. 12B, D. O. Thompson and D. E. Chimenti, eds. (Plenum Press, New York, 1993), pp. 1717–1726.
23. R. Bracewell, *The Fourier Transform and Its Applications* (Chap. 12) (McGraw-Hill, New York, 1965).
24. P. H. Rodgers and A. L. Van Buren, An exact expression for the Lommel diffraction integral, *J. Acoust. Soc. Am.* **55:**724–728 (1974).
25. M. Abramowitz and I. A. Stegun, *Handbook of Mathematical Functions* (Chap. 9) (Dover, New York, 1965).
26. R. B. Thompson and T. A. Gray, Range of applicability of inversion algorithms, in *Review of Progress in Quantitative NDE*, Vol. 1, D. O. Thompson and D. E. Chimenti, eds. (Plenum Press, New York, 1982), pp. 233–249.
27. R. B. Thompson and E. F. Lopes, The effects of focusing and refraction on Gaussian ultrasonic beams, *J. Nondestr. Eval.* **4:**107 (1984).
28. B. P. Newberry and R. B. Thompson, A paraxial theory for the propagation of ultrasonic beams in anisotropic solids, *J. Acoust. Soc. Am.* **85:**2290–2300 (1989).
29. K. Y. Han, R. B. Thompson, F. J. Margetan, and J. H. Rose, Relationship between ultrasonic noise and macrostructure of titanium alloys, in *Review of Progress in Quantitative NDE*, Vol. 12, D. O. Thompson and D. E. Chimenti, eds. (Plenum Press, New York, 1993), pp. 1743–1750.
30. J. M. M. Pinkerton, A pulse method for the measurement of ultrasonic absorption in liquids: Results for water, *Nature* **160:**128 (1947).
31. Yan Li and R. B. Thompson, Relations between elastic constants C_{ij} and texture parameters for hexagonal materials, *J. Appl. Phys.* **67**(5):2663–2665 (1990).

32. R. B. Thompson, J. F. Smith, S. S. Lee, and G. C. Johnson, Comparison of ultrasonic and X-ray determinations of texture in thin Cu and Al plates, *Metall. Trans. A* **20A:**2431–2447 (1989).
33. J. A. Ogilvy, Ultrasonic beam profiles and beam propagation in an austenitic weld using a theoretical ray tracing model, *Ultrasonics* **24:**337 (1986).
34. F. J. Margetan, R. B. Thompson, and I. Yalda-Mooshabad, Modeling ultrasonic microstructural noise in titanium alloys, in *Review of Progress in Quantitative NDE*, Vol. 12B, D. O. Thompson and D. E. Chimenti, eds. (Plenum Press, New York, 1993), pp. 1735–1742.
35. F. J. Margetan, R. B. Thompson, and I. Yalda-Mooshabad, Estimating ultrasonic signal-to-noise ratios for inspections of cylindrical billets, in *Review of Progress in Quantitative NDE*, Vol. 13B, D. O. Thompson and D. E. Chimenti, eds. (Plenum Press, New York, 1994), pp. 1737–1744.